

The Absolute Nodal Coordinate Formulation

Johannes Gerstmayr, Alexander Humer, Peter Gruber
and Karin Nachbagauer

Abstract The key idea of the absolute nodal coordinate formulation (ANCF) is to use slope vectors in order to describe the orientation of the cross-section of structural mechanics components, such as beams, plates or shells. This formulation relaxes the kinematical assumptions of Bernoulli–Euler and Timoshenko beam theories and enables a deformation of the cross-sections. The present contribution shows how to create 2D and 3D structural finite elements based on the ANCF by employing different sets of slope vectors for approximating the cross-sections’ orientation. A specific aim of this chapter is to present a unified notation for structural mechanics and continuum mechanics ANC formulations. Particular focus is laid on enhanced formulations for such finite elements that circumvent severe issues like Poisson or shear locking. The performance of these elements is evaluated and a detailed assessment comprising the convergence order, the number of iterations, and Jacobian updates for large deformation benchmark problems is provided.

1 Introduction

In a world with an increasing amount of automation, mobility, adaptive structures, and miniaturized systems, the modeling and simulation of flexible multibody systems gains importance. Large deformation of some components can significantly influence

J. Gerstmayr (✉)
Leopold-Franzens-Universität Innsbruck, Technikerstraße 13,
6020 Innsbruck, Austria
e-mail: johannes.gerstmayr@uibk.ac.at

A. Humer · P. Gruber
Linz Center of Mechatronics GmbH, Altenberger Straße 69, 4040 Linz, Austria

A. Humer
Johannes Kepler University, Altenberger Straße 69, 4040 Linz, Austria

K. Nachbagauer
University of Applied Sciences Upper Austria, Stelzhamerstraße 23,
4600 Wels, Austria

the behavior of the flexible multibody system. Examples are the dynamics of thin rotor blades, transportation of sheets or strips, various kinds of cables, wires, and tires.

There are several possibilities to study the dynamic behavior of slender structures. A convenient way to model large deformations of beam-like structures is to combine several beams described by the floating frame of reference formulation with an individual frame for each beam. As soon as the number of beams becomes larger, the solution of geometrically nonlinear problems converges to the solution of nonlinear beam formulations, see Gerstmayr and Irschik (2003) and Dibold et al. (2009). The floating frame approach has drawbacks like inappropriate modeling of nonlinearities for geometric stiffening and slow convergence and it cannot be extended to shells. Furthermore, the equations of motion as well as the constraint conditions for pairwise interconnection of beams become tedious. In finite element codes, large deformation structural finite elements based on the large rotation vector formulation of Simo and Vu-Quoc (1988) are available for studying the dynamics of thin structures. These elements require special time integration methods for stable long-term dynamic simulations.

In the present chapter, we focus on beam finite elements based on the absolute nodal coordinate formulation. Specifically, the focus of this chapter lies on a class of thin beam finite elements, based on the Bernoulli–Euler beam theory, and a class of thick beam finite elements, which include shear and cross-section deformation. This chapter provides a brief overview of existing absolute nodal coordinate (ANC) formulations, relations to other modeling techniques for large deformation beam finite elements, details on the formulation and implementation of the equations of motion, and some representative numerical tests that show the order of convergence, the performance and the stability of ANC beam finite elements.

1.1 ANCF—Basic Ideas

This section aims to highlight various basic ideas for ANC finite elements. For a recent review article on ANCF, which provides important references, see Gerstmayr et al. (2013b). We like to emphasize that some of the subsequent ideas do not apply to every ANC finite element published in the literature. In addition to that, there is no general definition whether to call a finite element ANC element, or not.

The first, and probably most widely accepted, idea is that ANC finite elements are based on slope vectors¹ rather than rotation parameters such as Euler angles or Euler parameters. Rotational parameters can immediately lead to a numerically induced blow up of the total energy in a conservative flexible multibody system, see the examples section of this chapter as well as the classical literature on 3D nonlinear beam formulations of the 1980s and 1990s, see Simo and Vu-Quoc (1988). As an advantage of the ANCF, slope vectors can be interpolated in space and time in

¹For an example of a slope vector, see $\mathbf{x}_{,\xi}$, $\mathbf{x}_{,\eta}$ or $\mathbf{x}_{,\zeta}$ in Fig. 2.

the same way as displacements, which does not lead to well-known problems of interpolation of rotations. As a disadvantage, the slope vectors are stiffly constrained to the nearly-rigid-body motion of the cross-section, which can cause high-frequency dynamics behavior.

As a result of a pure displacement (or displacement gradient) interpolation in space, ANC finite elements usually employ a constant mass matrix. This can lead to simpler implementation and computational efficiency. The straightforward kinematic description of the motion of each point of the beam makes an extension to advanced kinematics descriptions (such as ALE) or to multi-physics coupling much easier, see Pechstein and Gerstmayr (2013).

From the computational point of view, ANC finite elements are solved according to a Total Lagrangian (TL) scheme. This means, that no incremental (or co-rotational) formulation is utilized, which is sometimes applied in formulations based on rotational parameters.

ANC finite elements shall be capable of large deformations (in comparison to structural finite elements based on the floating frame of reference formulation) and can even be applied to (moderately) large strains. Specifically, in some sort of ANC finite elements, 3D continuum mechanics material laws can be directly applied, which makes this formulation attractive, e.g., for rubber-like materials, see Irschik and Gerstmayr (2009a).

The original shear and cross-section deformable ANC finite elements relax the assumptions of the classical Bernoulli–Euler and the Timoshenko beam theory, in the sense that the cross-section is not rigid any longer. As a consequence, the shrinkage of parts of the cross-section due to elongation can be modeled, which has many applications, e.g., in rolling processes.

In the case of so-called fully parametrized ANC finite elements, which use three slope vectors for the definition of the orientation of the cross-section, an interconnection of finite elements at any angle is possible without the need of constraint conditions, see Sugiyama et al. (2003).

There is a general transformation of the NURBS-based geometry of slender structures to ANC finite elements, which allows the direct computation of CAD geometry without the need for an intermediate discretization, see Lan and Shabana (2010a, b).

1.2 ANCF—Short Summary

There exist a vast amount of structural finite elements in the literature. Many of the proposed structural finite elements have specific objectives and purposes. Among other things, ANC finite elements have been designed for simulation of the dynamics of flexible multibody systems consisting of structural components. In this context, the term “structural” is used in order to distinguish such elements from conventional solid finite elements.

In one of the earliest papers on ANCF, Escalona et al. (1998) proposed a polynomial interpolation of the position of the beam axis for the computation

of the deformation energy, the kinetic energy and the mass matrix. In the latter paper, the authors used a planar Bernoulli–Euler beam theory, using a cubic interpolation along the axis of the beam finite element. A co-rotational frame is defined, which is spanned by the end points of the beam finite element, in order to compute the strain energy. However, the mass matrix becomes constant and the formulation can be implemented very efficiently. In order to extend the latter idea, it is possible to use cross-section slope vectors, see Yakoub and Shabana (2001), and to use a similar co-rotational linearization, see, e.g., Gerstmayr (2009).

The absolute nodal coordinate formulation facilitates the application of constitutive relations on the continuum mechanics level, therefore, almost arbitrary material laws as well as large strain formulations can be incorporated in a straightforward manner. The classical large deformation beam finite elements, which have been proposed by Simo (1985) and Simo and Vu-Quoc (1986c), are based on a strain energy which is a quadratic function of generalized strain measures such as axial strain or curvature. These strain measures can be interpreted in terms of continuum mechanics quantities, see Irschik and Gerstmayr (2009b), however, the ANCF allows for a much simpler realization of nonlinear, e.g., hyperelastic, material laws, see Irschik and Gerstmayr (2009a).

There are other approaches than ANC finite elements for the combination of continuum mechanics with structural finite elements, see Frischkorn and Reese (2012) for a recent work on beams modeled with hexahedrals. The slope vectors in the ANCF can be directly related to well-known director based methods, if constraints are applied to the length of the slopes vectors and for the orthogonality of the slope vectors. Applying constraints on a fully parametrized ANC beam finite element is in line with the approach proposed by Betsch and Steinmann (2003), see the corresponding chapter in this book. Furthermore, the latter approach is based on the geometrically exact beam formulation of Simo (1985).

There is one important group of so-called fully parametrized ANC finite elements. The term ‘fully parameterized’ indicates that all nine components of the spatial deformation gradient (four in the planar case) are used as coordinates in each node. Using these coordinates, it is possible to interconnect ANC finite elements with slope discontinuities without any constraint equations, see Sugiyama et al. (2003). In this chapter, a specific focus is laid on so-called gradient-deficient ANC finite elements, which means that less slope vectors are used than in the fully parametrized case.

There are several issues concerning the ANCF, which are not discussed in detail in the present chapter. The idea of using slopes as nodal degrees of freedom has been extended to plates, see Mikkola and Shabana (2003), resp. shells and general 3D solids, see Olshevskiy et al. (2013). In the present chapter, we only discuss planar and spatial ANC beam finite elements. The continuum mechanics formulation, which is frequently used for the computation of the elastic forces in ANCF, is well suited for the modeling of nonlinear elastic material, see Irschik and Gerstmayr (2011), or inelastic material behavior, see Sugiyama and Shabana (2004) and Gerstmayr and Matikainen (2006). The latter topics are not addressed in the present chapter.

2 General Formulation of ANC Beam Elements

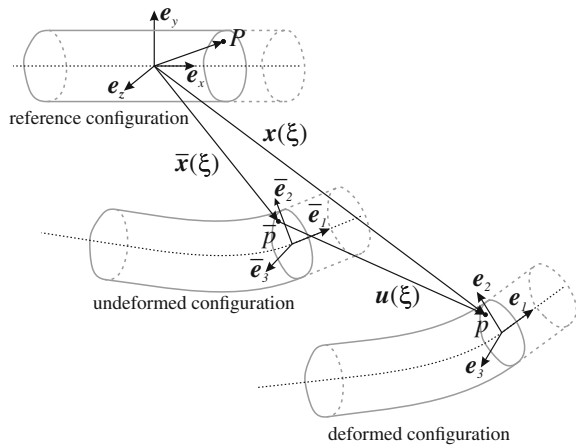
2.1 Kinematics of ANC Beam Elements

In the present section, the kinematic preliminaries describing the deformation of beams are introduced. Throughout the following sections, we employ a direct tensor notation or tensor components where appropriate. Einstein’s notion of summation over repeated indices is used for the sake of brevity. The scalar product of two vectors is given as $\mathbf{a}^T \mathbf{b} = a_i b_i$. The composition of two tensors and the linear mapping of a vector by a tensor read $\mathbf{A}\mathbf{A}^{-1} = \mathbf{I}$ and $\mathbf{A}\mathbf{b} = A_{ij}b_j$, respectively. The double contraction of tensors is indicated by a colon, e.g., the inner product of second-order tensors, i.e., $\mathbf{A} : \mathbf{B} = \text{tr}(\mathbf{A}^T \mathbf{B}) = A_{ij}B_{ij}$; the product of a fourth- and a second-order tensor is defined as ${}^4\mathbf{C} : \mathbf{A} = C_{ijkl}A_{kl}$. For the tensor product of two vectors, we use the notation $\mathbf{a} \otimes \mathbf{b} = a_i b_j$.

Regardless of whether structural finite elements as beams and plates or conventional solid elements are considered, large deformation problems in continuum mechanics require an exact representation of the geometry of deformation. As is customary in solid mechanics, a reference configuration is introduced which primarily serves the purpose of identifying a body’s material points. In the material or Lagrangian representation employed subsequently, the field variables are functions of the material points, or rather, their positions in the reference configuration. In order to avoid curvilinear coordinates, the reference configuration—not necessarily occupied by the body in the course of deformation—is a straight beam whose axis is aligned with the x -axis of some fixed Cartesian frame $\{\mathbf{e}_x, \mathbf{e}_y, \mathbf{e}_z\}$. Let (ξ, η, ζ) denote the (straight) referential coordinates, see Fig. 1, such that the position of some point P is identified by the vector $\boldsymbol{\xi}$,

$$\boldsymbol{\xi} = \xi \mathbf{e}_x + \eta \mathbf{e}_y + \zeta \mathbf{e}_z. \tag{1}$$

Fig. 1 Important geometrical definitions for ANC elements



In general, the undeformed beam can be curved and arbitrarily oriented relative to the previously introduced fixed frame. The undeformed configuration, relative to which the deformation is measured, therefore has to be distinguished from the reference configuration. The position of the material point P in the undeformed configuration is denoted by $\bar{\mathbf{x}}$, whose coordinates $(\bar{x}, \bar{y}, \bar{z})$ relative to the fixed frame are referred to as material coordinates subsequently:

$$\bar{\mathbf{x}} = \bar{x}\mathbf{e}_x + \bar{y}\mathbf{e}_y + \bar{z}\mathbf{e}_z. \quad (2)$$

The position in the undeformed state is related to the current position in the deformed configuration \mathbf{x} by means of the displacement vector \mathbf{u} , i.e.,

$$\mathbf{x} = \bar{\mathbf{x}} + \mathbf{u} = x\mathbf{e}_x + y\mathbf{e}_y + z\mathbf{e}_z. \quad (3)$$

The position vector to a material point of the beam's axis in undeformed configuration is defined as $\bar{\mathbf{r}}$ whereas in deformed configuration it reads \mathbf{r} .

Besides the idea of cross-sectional stress resultants, restrictions concerning the deformation of the beam's cross-section are a key ingredient enabling a reduction of a 3D problem to a 1D problem of a beam. All the beam finite elements discussed subsequently can be considered as more or less special cases of a single set of kinematic assumptions: Cross-sections, initially plane and perpendicular to the beam's axis in the undeformed configuration, remain plane in the course of deformation. In contrast to conventional formulations, however, we want to allow the cross-sections to change their size and shape, i.e., a constant in-plane stretch and shearing. Timoshenko's hypothesis would be recovered by prohibiting the latter; the classical assumption for slender structures attributed to Bernoulli and Euler would be obtained by further restricting that the cross-sections remain perpendicular to the beam's axis during deformation.

In the most general case considered herein, the position of the material point P can therefore be expressed in terms of the axis' initial and current position, i.e., $\bar{\mathbf{r}}$ and \mathbf{r} , respectively, as

$$\mathbf{x} = \mathbf{r} + \mathbf{A}(\bar{\mathbf{x}} - \bar{\mathbf{r}}) + \mathbf{u}_{cs}, \quad (4)$$

where \mathbf{u}_{cs} denotes the in-plane deformation of the cross-sections and the second-order tensor \mathbf{A} represents the rotation of the local frame in P from the undeformed to the deformed configuration:

$$\mathbf{A} = \mathbf{e}_i \otimes \bar{\mathbf{e}}_i. \quad (5)$$

The notions of bending and shear deformation in beam theories are intrinsically related to body-local directions. In order to specify the strain measures the subsequent formulations are based on, we therefore need to specify local frames in the beam's configurations used in the analysis. As the beam is straight in the reference configuration, we choose the associated local frame in the directions of the global Cartesian frame $\{\mathbf{e}_{\text{ref},1} = \mathbf{e}_x, \mathbf{e}_{\text{ref},2} = \mathbf{e}_y, \mathbf{e}_{\text{ref},3} = \mathbf{e}_z\}$. Expressing the position in the undeformed configuration in terms of the referential coordinates, $\bar{\mathbf{x}} = \bar{\mathbf{x}}(\xi, \eta, \zeta)$,

the corresponding local (cross-section) frame may be defined in dependence of the lateral slope vectors $\bar{\mathbf{x}}_{,\eta}$ and $\bar{\mathbf{x}}_{,\zeta}$. Under the convenient assumption that the undeformed configuration is chosen such that $\bar{\mathbf{x}}_{,\eta}$ and $\bar{\mathbf{x}}_{,\zeta}$ are perpendicular at every $\bar{\mathbf{x}}$, the definition of the local frame $(\bar{\mathbf{e}}_1, \bar{\mathbf{e}}_2, \bar{\mathbf{e}}_3)$ reads

$$\bar{\mathbf{e}}_1 = \frac{\bar{\mathbf{x}}_{,\eta} \times \bar{\mathbf{x}}_{,\zeta}}{\|\bar{\mathbf{x}}_{,\eta} \times \bar{\mathbf{x}}_{,\zeta}\|}, \quad \bar{\mathbf{e}}_2 = \frac{\bar{\mathbf{x}}_{,\eta}}{\|\bar{\mathbf{x}}_{,\eta}\|}, \quad \bar{\mathbf{e}}_3 = \frac{\bar{\mathbf{x}}_{,\zeta}}{\|\bar{\mathbf{x}}_{,\zeta}\|}. \quad (6)$$

Apparently, $\bar{\mathbf{e}}_1$ is perpendicular to the undeformed cross-section, whereas $\bar{\mathbf{e}}_2$ and $\bar{\mathbf{e}}_3$ lie within and are perpendicular to each other. The local frame is orthonormal and independent of the local position within the cross-section. Concerning the deformed configuration we proceed in a similar way, but here the lateral slope vectors are, in general, no more perpendicular. Let $\mathbf{x} = \mathbf{x}(\xi, \eta, \zeta)$, then the local frame $(\mathbf{e}_1, \mathbf{e}_2, \mathbf{e}_3)$ is given by

$$\mathbf{e}_1 = \frac{\mathbf{x}_{,\eta} \times \mathbf{x}_{,\zeta}}{\|\mathbf{x}_{,\eta} \times \mathbf{x}_{,\zeta}\|}, \quad \mathbf{e}_2 = \frac{\mathbf{x}_{,\zeta} \times (\mathbf{x}_{,\eta} \times \mathbf{x}_{,\zeta})}{\|\mathbf{x}_{,\zeta} \times (\mathbf{x}_{,\eta} \times \mathbf{x}_{,\zeta})\|}, \quad \mathbf{e}_3 = \frac{\mathbf{x}_{,\zeta}}{\|\mathbf{x}_{,\zeta}\|}. \quad (7)$$

Note, that the definition of the local frame is chosen arbitrarily, regarding its rotation about \mathbf{e}_1 . Particularly, $\mathbf{x}_{,\zeta}$ defines the rotation of the cross-section around \mathbf{e}_1 . Alternatively, $\mathbf{x}_{,\eta}$ could define the rotation of the cross-section, or a symmetric definition regarding the slope vectors could be built upon the polar decomposition—however, at higher computational costs.

With the local basis in the undeformed and the deformed configuration introduced, we can represent the respective rotation tensor from the reference to the undeformed configuration as

$$\bar{\mathbf{A}} = \bar{\mathbf{e}}_i \otimes \mathbf{e}_{\text{ref},i}, \quad (8)$$

and that from the reference to the deformed configuration becomes

$$\mathbf{A}\bar{\mathbf{A}} = \mathbf{e}_i \otimes \mathbf{e}_{\text{ref},i}. \quad (9)$$

2.1.1 Continuum Mechanics Formulation

Having provided the key ideas and assumptions concerning the geometry of deformation, the strain measures entering the constitutive equations are to be defined next. In the continuum mechanics formulation, Green's strain tensor is employed to measure the deformation,

$$\mathbf{E} = \frac{1}{2} (\mathbf{F}^T \mathbf{F} - \mathbf{I}), \quad (10)$$

where \mathbf{F} denotes the deformation gradient, which is expressed as

$$\mathbf{F} = \frac{\partial \mathbf{x}}{\partial \bar{\mathbf{x}}} = \frac{\partial \mathbf{x}}{\partial \xi} \frac{\partial \xi}{\partial \bar{\mathbf{x}}} = \frac{\partial \mathbf{x}}{\partial \xi} \left(\frac{\partial \bar{\mathbf{x}}}{\partial \xi} \right)^{-1}, \quad (11)$$

since we want to use the referential coordinates for the sake of simplicity. Green's strain—the change of the metric represented in the reference configuration—is consequently given by

$$\mathbf{E} = \frac{1}{2} \left(\frac{\partial \bar{\mathbf{x}}}{\partial \xi} \right)^{-T} \left\{ \left(\frac{\partial \mathbf{x}}{\partial \xi} \right)^T \frac{\partial \mathbf{x}}{\partial \xi} - \left(\frac{\partial \bar{\mathbf{x}}}{\partial \xi} \right)^T \left(\frac{\partial \bar{\mathbf{x}}}{\partial \xi} \right) \right\} \left(\frac{\partial \bar{\mathbf{x}}}{\partial \xi} \right)^{-1}. \quad (12)$$

In case of an initially straight beam, the undeformed configuration is typically chosen as the reference configuration, i.e., $\xi = \bar{\mathbf{x}}$. Accordingly, Green's strain tensor then reduces to the well-known representation

$$\mathbf{E} = \frac{1}{2} \left\{ \left(\frac{\partial \mathbf{x}}{\partial \xi} \right)^T \frac{\partial \mathbf{x}}{\partial \xi} - \mathbf{I} \right\}, \quad (13)$$

in which $\mathbf{I} = \mathbf{e}_{\text{ref},i} \otimes \mathbf{e}_{\text{ref},i}$ denotes the identity tensor.

While the choice of the above strain measure is natural within continuum theory, the structural mechanics formulation relies on the introduction of proper generalized strain measures which originate in the Cosserat theory of solids, which is described in what follows.

2.1.2 Structural Mechanics Formulation

Neglecting the in-plane deformation of cross-sections at first, a beam can be thought of as an elastic line with cross-sections attached to it. In the nonlinear rod model, the elastic line gets translated and stretched in the course of deformation; the cross-sections, which are represented by the local frames introduced above, undergo a rigid body rotation. The vector of generalized force strains describing both axial extension and shear deformation is the change of the derivatives of the axis's position vector with respect to the undeformed arc-length S :

$$\boldsymbol{\Gamma} = \frac{\partial \mathbf{r}}{\partial S} - \mathbf{A} \frac{\partial \bar{\mathbf{r}}}{\partial S}. \quad (14)$$

In order to compute the difference, the derivative in the deformed configuration is transformed into the local frame of the beam's undeformed configuration. Recalling that we want to express the involved field variables as functions of the referential coordinates, we use the relationship

$$dS = \sqrt{\left(\frac{\partial \bar{x}}{\partial \xi} \right)^2 + \left(\frac{\partial \bar{y}}{\partial \xi} \right)^2 + \left(\frac{\partial \bar{z}}{\partial \xi} \right)^2} d\xi = \left\| \frac{\partial \bar{\mathbf{r}}}{\partial \xi} \right\| d\xi \quad (15)$$

for rewriting the generalized force strains as

$$\boldsymbol{\Gamma} = \left\| \frac{\partial \bar{\mathbf{r}}}{\partial \xi} \right\|^{-1} \left(\frac{\partial \mathbf{r}}{\partial \xi} - \mathbf{A} \frac{\partial \bar{\mathbf{r}}}{\partial \xi} \right). \quad (16)$$

The definition of the generalized moment strains relies on the fundamental property of orthogonal tensors that

$$\mathbf{A} \mathbf{A}^T = \mathbf{I} \Rightarrow \frac{\partial \mathbf{A}}{\partial S} \mathbf{A}^T = -\mathbf{A} \frac{\partial \mathbf{A}^T}{\partial S} = - \left(\frac{\partial \mathbf{A}}{\partial S} \mathbf{A}^T \right)^T. \quad (17)$$

The vector of moment strains $\boldsymbol{\kappa}$ is the vector associated with the above skew-symmetric tensor such that the following identity holds for any vector \mathbf{v} ,

$$\boldsymbol{\kappa} \times \mathbf{v} = \left(\frac{\partial \mathbf{A}}{\partial S} \mathbf{A}^T \right) \mathbf{v}. \quad (18)$$

For an alternative representation of the generalized moment strains, the vector of twist and curvature \mathbf{k} is introduced,

$$\mathbf{k} = \frac{1}{2} \mathbf{e}_i \times \frac{\partial \mathbf{e}_i}{\partial S}, \quad (19)$$

which describes the change of the local basis along a material line,

$$\frac{\partial \mathbf{e}_i}{\partial S} = \mathbf{k} \times \mathbf{e}_i. \quad (20)$$

Likewise, the vector of the curvature and twist in the undeformed configuration is given by

$$\bar{\mathbf{k}} = \frac{1}{2} \bar{\mathbf{e}}_i \times \frac{\partial \bar{\mathbf{e}}_i}{\partial S}. \quad (21)$$

In terms of these vectors, the change of the local basis along the beam's axis can be written as

$$\frac{\partial \mathbf{A}}{\partial S} = \frac{\partial \mathbf{e}_i}{\partial S} \otimes \bar{\mathbf{e}}_i + \mathbf{e}_i \otimes \frac{\partial \bar{\mathbf{e}}_i}{\partial S} = (\mathbf{k} \times \mathbf{e}_i) \otimes \bar{\mathbf{e}}_i - \mathbf{e}_i \otimes (\bar{\mathbf{e}}_i \times \bar{\mathbf{k}}). \quad (22)$$

The product with the \mathbf{A}^T yields

$$\frac{\partial \mathbf{A}}{\partial S} \mathbf{A}^T = (\mathbf{k} \times \mathbf{e}_i) \otimes \mathbf{e}_i - \mathbf{e}_i \otimes (\bar{\mathbf{e}}_i \times \bar{\mathbf{k}}) \mathbf{A}^T = (\mathbf{k} \times \mathbf{e}_i) \otimes \mathbf{e}_i - \mathbf{e}_i \otimes (\mathbf{e}_i \times \mathbf{A} \bar{\mathbf{k}}), \quad (23)$$

where the identity $\mathbf{a} \times \mathbf{b} = (\mathbf{Aa} \times \mathbf{Ab})\mathbf{A}$ has been utilized. The skew-symmetry of the above tensor allows us to rewrite the product with some vector \mathbf{v} as

$$\left(\frac{\partial \mathbf{A}}{\partial S} \mathbf{A}^T \right) \mathbf{v} = (\mathbf{k} \times \mathbf{v}) - (\mathbf{A}\bar{\mathbf{k}} \times \mathbf{v}) = (\mathbf{k} - \mathbf{A}\bar{\mathbf{k}}) \times \mathbf{v}. \quad (24)$$

Comparing this result with the previous definition (18), we can immediately identify the simple representation of $\boldsymbol{\kappa}$ in terms of \mathbf{k} and $\bar{\mathbf{k}}$ as

$$\boldsymbol{\kappa} = \mathbf{k} - \mathbf{A}\bar{\mathbf{k}}. \quad (25)$$

2.2 Equations of Motion

Pursuing a finite element discretization, the equations of motion are discussed in their weak form. According to d'Alembert's principle in Lagrange's representation, the virtual work of the external forces is balanced by the sum of the virtual work of the internal forces, i.e., the variation of the strain energy, and the virtual work of the inertia forces

$$\delta W^{\text{inert}} + \delta W^{\text{int}} = \delta W^{\text{ext}}. \quad (26)$$

Similar to other beam formulations, the virtual work of external forces can be given in terms of products of concentrated forces and torques times virtual displacements and rotations, respectively. The virtual rotations need to be determined from the rotation tensor \mathbf{A} and consequently from the slope vectors involved, cf. (6)–(7). The virtual work of surface tractions and body forces is obtained from surface and volume integrals over their products with the corresponding virtual displacements.

The virtual work of the inertia forces is given by the volume integral over the beam's domain Ω in the following reference configuration:

$$\delta W^{\text{inert}} = \int_{\Omega} \rho_0 \ddot{\mathbf{u}}^T \delta \mathbf{u} dV, \quad (27)$$

where the variation of the displacement field is indicated by a δ and ρ_0 denotes the referential density. Regardless of the particular kinematic hypothesis employed, the key idea of absolute displacements being interpolated results in a constant mass matrix. This property underlies all ANC elements discussed subsequently, apart from the ANC-like formulation concerning the thin spatial beam element with torsional stiffness of Sect. 3.5.

2.2.1 Continuum Mechanics Formulation

The virtual work of the internal forces in the continuum mechanics formulation corresponds to what is known from the conventional continuum theory of solids. Accordingly, the second Piola–Kirchhoff stress tensor \mathbf{T} is work-conjugate to Green’s strain tensor:

$$\delta W^{\text{int}} = \int_{\Omega} \mathbf{T} : \delta \mathbf{E} dV. \quad (28)$$

In case of a linearly elastic material—in finite strain theory, such constitutive behavior is referred to as St. Venant–Kirchhoff material—the stress tensor is given as

$$\mathbf{T} = {}^4\mathbf{D} : \mathbf{E}, \quad (29)$$

in which ${}^4\mathbf{D}$ is the fourth-order tensor of elastic moduli. In the isotropic case, e.g., it contains two independent parameters, i.e., Young’s modulus E and Poisson’s ratio ν . From a computational point of view, the distinction between vectors and tensors and their components with respect to some particular basis has to be taken care of at this point. In the numerical implementation, one often prefers to represent all quantities in the common inertial frame of the reference configuration $\{\mathbf{e}_x, \mathbf{e}_y, \mathbf{e}_z\}$. When evaluating Green’s strain tensor (12), the components are usually given with respect to the inertial frame whereas the components of the tensor of elastic moduli refer to the local frame in the undeformed configuration $\{\bar{\mathbf{e}}_1, \bar{\mathbf{e}}_2, \bar{\mathbf{e}}_3\}$. Therefore, one must either represent the components of ${}^4\mathbf{D}$ in the inertial frame when evaluating the stresses, or, alternatively, transform the components of the strain tensor into the local frame of the undeformed configuration using the rotation tensor $\bar{\mathbf{A}}$:

$$[\bar{\mathbf{E}}] = [\bar{\mathbf{A}}]^T [\mathbf{E}] [\bar{\mathbf{A}}]. \quad (30)$$

In the above relation, we have introduced brackets in order to clearly distinguish between a tensor as an invariant object and its components relative to some tensorial basis. Subsequently, the components of the stress tensor can be determined from the constitutive equation (29), where a vector-matrix representation is typically employed for the sake of simplicity. Collecting the six independent components of both stress and strain tensor relative to the natural basis of the undeformed configuration $\{\bar{\mathbf{e}}_1, \bar{\mathbf{e}}_2, \bar{\mathbf{e}}_3\}$ in vectors,

$$\bar{\boldsymbol{\tau}} = [\bar{T}_{11}, \bar{T}_{22}, \bar{T}_{33}, \bar{T}_{23}, \bar{T}_{13}, \bar{T}_{12}]^T, \quad (31)$$

$$\bar{\boldsymbol{\varepsilon}} = [\bar{E}_{11}, \bar{E}_{22}, \bar{E}_{33}, 2\bar{E}_{23}, 2\bar{E}_{13}, 2\bar{E}_{12}]^T, \quad (32)$$

Equation (29) can be equivalently rewritten in terms of the 6×6 matrix $\bar{\mathbf{D}}_{\text{CM}}$ as

$$\bar{\boldsymbol{\tau}} = \bar{\mathbf{D}}_{\text{CM}} \bar{\boldsymbol{\varepsilon}}, \quad (33)$$

where $\bar{\mathbf{D}}_{\text{CM}}$ gathers all relevant components of the fourth-order tensor ${}^4\mathbf{D}$. In case of a linearly elastic, isotropic material, for instance, the matrix is given by

$$\bar{\mathbf{D}}_{\text{CM}} = \frac{E\nu^2}{(1+\nu)(1-2\nu)} \begin{bmatrix} 1-\nu & 1 & 1 & 0 & 0 & 0 \\ 1 & 1-\nu & 1 & 0 & 0 & 0 \\ 1 & 1 & 1-\nu & 0 & 0 & 0 \\ 0 & 0 & 0 & \frac{1-2\nu}{2} & 0 & 0 \\ 0 & 0 & 0 & 0 & \frac{1-2\nu}{2}k_2 & 0 \\ 0 & 0 & 0 & 0 & 0 & \frac{1-2\nu}{2}k_3 \end{bmatrix}, \quad (34)$$

where k_2 and k_3 denote shear correction factors that account for the non-uniform distribution of shear stresses within the beam's cross-section. Note that these correction factors may be different from well-known structural mechanics shear correction factors due to the specific integration over the cross-section in ANC finite elements. While the shear correction factors provided above enable a correct transverse shear stiffness, a correction for torsional stiffness is not accounted for in the present continuum mechanics formulation.

The components of the second Piola–Kirchhoff stress tensor $\bar{\mathbf{T}}$, which are collected in the vector $\bar{\boldsymbol{\tau}}$, need to be transformed back into the reference frame afterwards

$$[\mathbf{T}] = [\bar{\mathbf{A}}][\bar{\mathbf{T}}][\bar{\mathbf{A}}]^T. \quad (35)$$

With the stress tensor given, the variation of Green's strain tensor remains to be determined when evaluating the virtual work of the internal forces (28):

$$\delta\mathbf{E} = \frac{1}{2} \left(\frac{\partial \bar{\mathbf{x}}}{\partial \xi} \right)^{-T} \left\{ \left(\frac{\partial(\delta\mathbf{x})}{\partial \xi} \right)^T \frac{\partial \mathbf{x}}{\partial \xi} + \left(\frac{\partial \mathbf{x}}{\partial \xi} \right)^T \frac{\partial(\delta\mathbf{x})}{\partial \xi} \right\} \left(\frac{\partial \bar{\mathbf{x}}}{\partial \xi} \right)^{-1}. \quad (36)$$

2.2.2 Structural Mechanics Formulation

As opposed to the continuum mechanics formulation, the question of rational stress resultants that are conjugate to the previously introduced generalized strain measures is raised on a structural level. The internal forces and moments \mathbf{f} and \mathbf{m} , respectively, represent stress resultants that can be regarded as quantities obtained upon a static condensation of the stress distribution within the cross-section relative to the beam's axis. The present variational formulation of the strain energy relies on the ideas of Reissner (1972, 1973), Antman (1972) and Simo (1985) according to which the internal forces are conjugate to the generalized force strains and the internal moments to the generalized moment strains, respectively,

$$\delta W^{\text{int}} = \int_L \mathbf{f}^T \delta \boldsymbol{\Gamma} + \mathbf{m}^T \delta \boldsymbol{\kappa} d\xi, \quad (37)$$

where L denotes the length of the beam in the undeformed configuration. In the case of elastic material behavior, the constitutive equations for the cross-sectional forces and moments can be expressed as

$$\mathbf{f} = \mathbf{a}\boldsymbol{\Gamma} + \mathbf{c}^T \boldsymbol{\kappa}, \quad \mathbf{m} = \mathbf{b}\boldsymbol{\kappa} + \mathbf{c}\boldsymbol{\Gamma}, \quad (38)$$

with \mathbf{a} , \mathbf{b} and \mathbf{c} denoting second-order tensors of cross-sectional stiffnesses. Once again, the question of the respective basis of vectors and tensors involved needs to be addressed. The components of $\boldsymbol{\Gamma}$ and $\boldsymbol{\kappa}$ are typically available in the inertial frame that is used throughout the numerical analysis. The constitutive behavior (38), however, represents a locally linear behavior with a constant tangent stiffness that rotates with the beam in the course of deformation. Similar to the continuum mechanics approach, we have two options: one is determining the components of the material tensors relative to the inertial frame. Alternatively, the components of the generalized strains in the local frame of either the beam's undeformed or its deformed configuration are computed using the respective rotation tensor. Choosing the local frame in the undeformed configuration, the components of $\boldsymbol{\Gamma}$ and $\boldsymbol{\kappa}$ are transformed by means of

$$[\bar{\boldsymbol{\Gamma}}] = [\bar{\mathbf{A}}][\boldsymbol{\Gamma}], \quad [\bar{\boldsymbol{\kappa}}] = [\bar{\mathbf{A}}][\boldsymbol{\kappa}]. \quad (39)$$

Again, we can gather the stress resultants and the generalized strains in vectors in order to represent the material behavior by means of a matrix equation:

$$\bar{\boldsymbol{\tau}}_{\text{SM}} = \mathbf{D}_{\text{SM}} \bar{\boldsymbol{\epsilon}}_{\text{SM}} \quad (40)$$

with

$$\bar{\boldsymbol{\tau}}_{\text{SM}} = [\bar{f}_1, \bar{f}_2, \bar{f}_3, \bar{m}_1, \bar{m}_2, \bar{m}_3]^T, \quad \bar{\boldsymbol{\epsilon}}_{\text{SM}} = [\bar{\Gamma}_1, \bar{\Gamma}_2, \bar{\Gamma}_3, \bar{\kappa}_1, \bar{\kappa}_2, \bar{\kappa}_3]^T. \quad (41)$$

where \mathbf{D}_{SM} is the 6×6 cross-sectional stiffness matrix. In case of simple symmetric cross-sections, the coupling term disappears, i.e., $\mathbf{c} = \mathbf{0}$, and \mathbf{D}_{SM} becomes diagonal,

$$\mathbf{D}_{\text{SM}} = \text{diag} (EA, k_2 GA_2, k_3 GA_3, GJ_1, EI_2, EI_3), \quad (42)$$

with commonly used beam properties, i.e., the axial stiffness EA , corrected shear stiffnesses $k_{2,3} GA_{2,3}$, torsional rigidity GJ_1 and bending stiffnesses $EI_{2,3}$.

To this point, the deformation of the cross-sections \mathbf{u}_{cs} in Eq. (4) has not been addressed within the structural mechanics formulation. In conventional beam theories, the cross-sections are usually assumed to be rigid, i.e., they only undergo a rotation relative to the undeformed configuration. Although such restriction has proven useful in many engineering applications, a significant change of the cross-sections size is inherent to certain problems as, e.g., rolling processes in metal processing. Among some of the ANC elements discussed subsequently, the parametrization facilitates including such deformation of the cross-sections' from a numerical point of view. For this purpose, the question of how to consistently augment the virtual work

of the internal forces in terms of appropriate strain measures and conjugate forces needs to be answered. A natural approach is to extend the structural mechanics formulation by the corresponding terms in the continuum mechanics formulation. Following Eq. (4), the deformation gradient is expressed as

$$\mathbf{F} = \frac{\partial}{\partial \bar{\mathbf{x}}} \{ \mathbf{r} + \mathbf{A} (\bar{\mathbf{x}} - \bar{\mathbf{r}}) \} + \mathbf{G}_{\text{cs}}, \quad (43)$$

where the displacement gradient \mathbf{G}_{cs} represents the additional contribution from the deformation of the cross-sections given by

$$\mathbf{G}_{\text{cs}} = \frac{\partial \mathbf{u}_{\text{cs}}}{\partial \bar{\mathbf{x}}}. \quad (44)$$

The definition of Green's strain (10) immediately reveals the coupling of the cross-sections' stretching and shearing with the conventional deformation allowed within Timoshenko's hypothesis. Subsequently, however, we introduce the key assumption that the in-plane deformation of the cross-sections does not interfere with the original structural mechanics formulation, or, in other words, the cross-section deformation is decoupled from generalized strain measures introduced above. Accordingly, only the in-plane components of the strain tensor (12), i.e.,

$$\bar{E}_{22} = \bar{\mathbf{e}}_2^T (\mathbf{E} \bar{\mathbf{e}}_2), \quad \bar{E}_{33} = \bar{\mathbf{e}}_3^T (\mathbf{E} \bar{\mathbf{e}}_3), \quad \bar{E}_{23} = \bar{\mathbf{e}}_3^T (\mathbf{E} \bar{\mathbf{e}}_2), \quad (45)$$

are regarded when augmenting the virtual work of the internal forces. The above requirement further implies that the cross-sections' deformation does not affect the generalized forces and moments of the structural mechanics formulation, which—from a continuum mechanics perspective—represent cross-sectional resultants of the stresses. In case of an elastic material, for instance, we have to stipulate $\nu = 0$ such that the conjugate stresses are given by

$$T_{22} = E \bar{E}_{22}, \quad T_{33} = E \bar{E}_{33}, \quad T_{23} = 2G \bar{E}_{23}, \quad (46)$$

where E and G denote the Young's modulus and the shear modulus, respectively. The additional term in the virtual work of the internal forces consequently reads

$$\delta W_{\text{cs}}^{\text{int}} = \int_{\Omega} E (\bar{E}_{22} \delta \bar{E}_{22} + \bar{E}_{33} \delta \bar{E}_{33}) + 2G \bar{E}_{23} \delta \bar{E}_{23} dV. \quad (47)$$

If the in-plane strains are distributed uniformly within the cross-sections, the above relation simplifies to

$$\delta W_{\text{cs}}^{\text{int}} = \int_L EA (\bar{E}_{22} \delta \bar{E}_{22} + \bar{E}_{33} \delta \bar{E}_{33}) + 2GA \bar{E}_{23} \delta \bar{E}_{23} d\xi, \quad (48)$$

where the axial and shear stiffness have been introduced, which further connects the cross-sections' deformation to the structural mechanics formulation. The total variation of the internal forces is obtained by adding the contribution from the cross-sections (48) to the conventional expression for the virtual work of the internal forces (37):

$$\delta W_{\text{tot}}^{\text{int}} = \delta W^{\text{int}} + \delta W_{\text{cs}}^{\text{int}}. \quad (49)$$

Before we proceed with the derivations, a few comments on the cross-sections' deformation seem to be appropriate. The numerous assumptions needed to eventually arrive at the simple expression (48) may appear restrictive to such an extent that the general applicability of the proposed formulation is questionable at best. The answer to that question is twofold: indeed but deliberately. The extension of the structural mechanics formulation for beams is not meant to contain all features of deformation a structure can be subjected to. It is specifically aimed at problems in which uniform in-plane stretch and shearing are relevant—as in the examples mentioned above—but the assumptions underlying the structural mechanics formulation are sufficient otherwise. That is to say, including the cross-sectional deformation widens the scope of applicability of the efficient structural mechanics formulation. In problems showing a more complex state of deformation, for which the coupling of in-plane and out-of-plane deformation cannot be neglected, the continuum mechanics formulation needs to be resorted to.

From a numerical point of view, the expressions to be evaluated in the general case of a beam that is arbitrarily curved in its undeformed configuration are relatively complicated since both the generalized strains and conjugate forces of the structural mechanics approach and the components of the strain tensor and the conjugate stresses of the continuum mechanics formulation are required. For an initially straight beam, however, the terms related to the cross-sectional deformation simplify significantly. In this case, the relevant components of Green's strain tensor with respect to the global frame are given by

$$E_{\eta\eta} = \frac{1}{2} \left(\frac{\partial \mathbf{x}}{\partial \eta} \frac{\partial \mathbf{x}}{\partial \eta} - 1 \right), \quad E_{\zeta\zeta} = \frac{1}{2} \left(\frac{\partial \mathbf{x}}{\partial \zeta} \frac{\partial \mathbf{x}}{\partial \zeta} - 1 \right), \quad E_{\eta\zeta} = \frac{1}{2} \frac{\partial \mathbf{x}}{\partial \eta} \frac{\partial \mathbf{x}}{\partial \zeta}. \quad (50)$$

Some of the ANC elements discussed subsequently are based on the interpolation of the derivatives contained in the above relations which greatly facilitates the evaluation of the strains related to the cross-sectional deformation.

2.3 Numerical Interpolation

The fundamental idea of ANCF is the direct interpolation of positions and position gradients with respect to the global frame—therefore, absolute—using positions and position gradients of a finite number of points, i.e., the nodes. Accordingly, the position vector—or rather, its components with respect to the global frame—of a

beam's material point is represented by a Ritz approach as

$$\mathbf{x}(\boldsymbol{\xi}, t) = \mathbf{S}(\boldsymbol{\xi})\mathbf{q}(t), \quad \mathbf{x} \in \mathbb{R}^m \quad (51)$$

where \mathbf{q} denotes the vector of n generalized coordinates and \mathbf{S} is the $m \times n$ matrix of interpolation or shape functions, which is briefly referred to as shape function matrix. Naturally, the same representation is used for the position field in the undeformed configuration,

$$\bar{\mathbf{x}}(\boldsymbol{\xi}) = \mathbf{S}(\boldsymbol{\xi})\bar{\mathbf{q}}. \quad (52)$$

Regarding both formulation and implementation, it should be mentioned that it is more or less a matter of taste of whether absolute nodal positions or displacements are utilized as generalized coordinates. Employing a Galerkin projection, the variation of the position is contained in the same function space as the position vector itself, i.e., we use the same shape function matrix

$$\delta\mathbf{x}(\boldsymbol{\xi}) = \mathbf{S}(\boldsymbol{\xi})\delta\mathbf{q}. \quad (53)$$

2.4 Overview of Different ANC Finite Elements

In the absolute nodal coordinate formulation, the design of finite elements is based on the choice of nodal degrees of freedom (coordinates).

In most ANC finite elements, the nodal coordinates consist of position or displacement coordinates as well as the corresponding derivatives with respect to the referential coordinates (ξ, η, ζ) .

Figure 2 shows selected 2D and 3D ANC finite elements. As a minimum, one axial slope vector is employed in order to create a Bernoulli–Euler beam finite elements, see Fig. 2a, b. Another case is retrieved, if all components of the gradient at each node are used to define shear and cross-section deformable ANC finite elements, also denoted as fully parametrized, see Fig. 2c, d. The term ‘fully parametrized’ is used, because all components of the gradient at the nodal positions are parametrized by three nodal slope vectors.

The coordinates of two- and three-noded beam finite elements according to Eq. (51) can be given in the general form,

$$\begin{aligned} \mathbf{q}^{(2 \text{ node})} &= \left[\mathbf{q}^{(1)T} \quad \mathbf{q}^{(2)T} \right]^T, \quad \text{and} \\ \mathbf{q}^{(3 \text{ node})} &= \left[\mathbf{q}^{(1)T} \quad \mathbf{q}^{(2)T} \quad \mathbf{q}^{(3)T} \right]^T. \end{aligned} \quad (54)$$

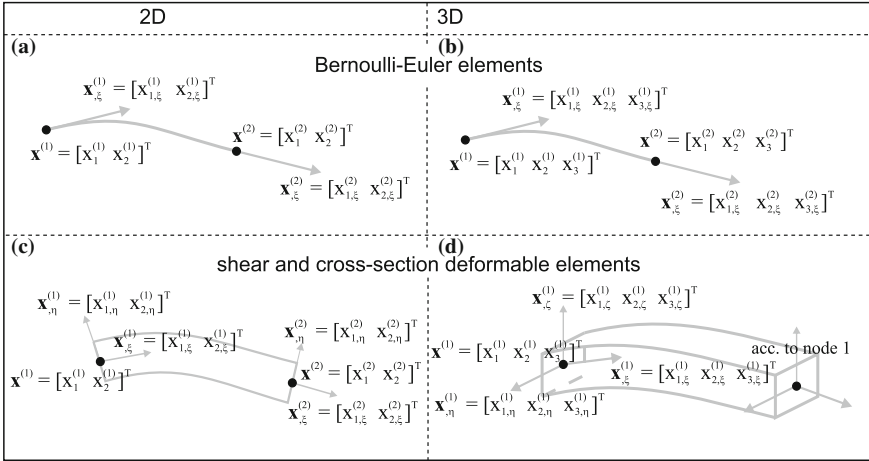


Fig. 2 Overview of some basic ANC finite elements. **a** 8 DOF, planar ANC finite element, **b** 12 DOF, spatial ANC finite element, **c** 12 DOF, planar ANC finite element with shear and cross-section deformation, **d** 24 DOF, spatial ANC finite element with shear and cross-section deformation

in which $\mathbf{q}^{(i)T}$ represents the nodal coordinates of the i -th node. Following the original idea of the ANCF, a fully parametrized set of nodal position and slope vectors has been utilized,

$$\mathbf{q}_{ip}^{(j)} = \left[\mathbf{x}^{(j)T} \quad \mathbf{x}_{,\xi}^{(j)T} \quad \mathbf{x}_{,\eta}^{(j)T} \quad \mathbf{x}_{,\zeta}^{(j)T} \right]^T. \quad (55)$$

The vector $\mathbf{x}^{(j)}$ represents the current position of the node j of the beam finite element. Note that the nodal coordinates of Eq. (55) are comprised of the position and three slope vectors which represent the deformation gradient.

In order to efficiently model ANC beam finite elements based on the Bernoulli–Euler theory, so-called gradient-deficient nodal coordinates are utilized, which means that not all components of the gradient are employed in the nodal coordinates,

$$\mathbf{q}_{axial}^{(j)} = \left[\mathbf{x}^{(j)T} \quad \mathbf{x}_{,\xi}^{(j)T} \right]^T. \quad (56)$$

In case of ANC beam finite elements which cover the Timoshenko beam theory, gradient-deficient nodal coordinate that which do not contain the axial slope vector are frequently used

$$\mathbf{q}_{cross-section}^{(j)} = \left[\mathbf{x}^{(j)T} \quad \mathbf{x}_{,\eta}^{(j)T} \quad \mathbf{x}_{,\zeta}^{(j)T} \right]^T. \quad (57)$$

3 ANC Finite Elements Based on the Bernoulli-Euler Condition

In this section, the 2D and 3D formulations of thin beam (or cable) finite elements based on the ANCF are discussed. The original formulations of 2D Bernoulli–Euler ANC beam finite elements have been developed by Shabana and Schwertassek (1997) and later on by Berzeri and Shabana (2002). In the present section, an extended formulation is presented for 2D and 3D thin beams, which follows the works of Gerstmayr and Shabana (2006), Gerstmayr and Irschik (2008) and Gruber et al. (2013).

3.1 Kinematics of Thin ANC Beam Finite Elements

For notational convenience, the derivative of a quantity with respect to the axial coordinate ξ is subsequently abbreviated as

$$\frac{\partial ()}{\partial \xi} = ()'. \quad (58)$$

The two-noded planar element has eight degrees of freedom, see Fig. 2a. For such beam element, the position (or displacement) of its axis can be interpolated by two third-order polynomials in ξ ,

$$\mathbf{x}^{2D} = \begin{bmatrix} x_1^{2D} \\ x_2^{2D} \end{bmatrix} = \begin{bmatrix} a_0 + a_1\xi + a_2\xi^2 + a_3\xi^3 \\ b_0 + b_1\xi + b_2\xi^2 + b_3\xi^3 \end{bmatrix}. \quad (59)$$

The coefficients a_i and b_i are determined by requiring that the generalized degrees of freedom \mathbf{q}^{2D} represent components of the nodal positions (or displacements) and slope vectors. Using third-order polynomials also for the interpolation of the slope vectors, we obtain the shape functions S_i ,

$$\begin{aligned} S_1 &= \frac{1}{2} - \frac{3}{4}\xi + \frac{1}{4}\xi^3, & S_2 &= \frac{L}{8} (1 - \xi - \xi^2 + \xi^3), \\ S_3 &= \frac{1}{2} + \frac{3}{4}\xi - \frac{1}{4}\xi^3, & S_4 &= \frac{L}{8} (-1 - \xi + \xi^2 + \xi^3). \end{aligned}$$

which are gathered in the shape function matrix \mathbf{S}_m as

$$\mathbf{x}^{2D} = [S_1\mathbf{I} \quad S_2\mathbf{I} \quad S_3\mathbf{I} \quad S_4\mathbf{I}]\mathbf{q}^{2D} = \mathbf{S}_m\mathbf{q}^{2D}, \quad (60)$$

in which \mathbf{I}^{2D} is the 2×2 unit matrix.

In addition to the thin planar ANC beam element, two formulations for spatial (3D) thin ANC finite elements exist. The simplest spatial element considers bending

and axial stretch only, see Gerstmayr and Shabana (2006), and thus can only be used to model cable problems, whereas an extended formulation for spatial beam elements can also handle torsion. The latter extends the idea of Dmitrochenko and Pogorelov (2003) in order to prevent from singularities, see Gruber et al. (2013) or Sect. 3.5.

For thin spatial beams, the polynomial interpolation of the position reads

$$\mathbf{x} = \begin{bmatrix} x_1 \\ x_2 \\ x_3 \end{bmatrix} = \begin{bmatrix} a_0 + a_1\xi + a_2\xi^2 + a_3\xi^3 \\ b_0 + b_1\xi + b_2\xi^2 + b_3\xi^3 \\ c_0 + c_1\xi + c_2\xi^2 + c_3\xi^3 \end{bmatrix}. \quad (61)$$

Again, the coefficients a_i , b_i and c_i are chosen such that the generalized coordinates \mathbf{q} correspond to the components of the position (or displacement) and slope vectors at the nodes. For a compact representation of the relation between the position vector and the element coordinates, the shape functions can be collected in the shape function matrix,

$$\mathbf{x} = [S_1\mathbf{I} \quad S_2\mathbf{I} \quad S_3\mathbf{I} \quad S_4\mathbf{I}]\mathbf{q} = \mathbf{S}_m\mathbf{q}. \quad (62)$$

Note that we will not distinguish between planar (2D) and spatial vectors in the following since most mathematical operations are identical. In the planar case, the vector product (\times) is understood as the product of two spatial vectors that represent the embedding of the planar ones in the 3D space.

3.2 Virtual Work of Elastic Forces for Thin Beams Without Torsional Stiffness

In thin ANC beam finite elements, only a structural mechanics formulation exists for the definition of the elastic forces, while in the thick ANC beam finite elements, both a continuum mechanics and structural mechanics formulations are available for the computation of the elastic forces.

3.2.1 Bending and Axial Strain

In the present section, the kinematics and the strain energy of a planar Bernoulli–Euler beam undergoing large rigid body motions and large deformations (but small strains) is investigated. In order to keep this section simple, the planar beam formulation is written for an initially straight and undeformed beam, assuming that the undeformed configuration is identical to the reference configuration (beam aligned along \mathbf{e}_x axis).

The kinematics of the beam element is according to Fig. 1. In a planar Bernoulli–Euler beam, Eq. (4) reduces to

$$\mathbf{x}(\xi, \eta) = \mathbf{r}(\xi) + \eta \mathbf{e}_2(\xi). \quad (63)$$

The local basis, which is rigidly attached to the cross-section of the beam in current configuration, is simply defined within the relations

$$\mathbf{e}_1 = \frac{1}{\|\mathbf{r}'\|} \frac{\partial \mathbf{r}}{\partial \xi}, \quad \mathbf{e}_1^T \mathbf{e}_2 = 0, \quad \mathbf{e}_2^T \mathbf{e}_z = 0, \quad \text{and} \quad \mathbf{e}_3 = \mathbf{e}_z. \quad (64)$$

The derivative of the position vector \mathbf{x} with respect to ξ is given by

$$\mathbf{x}' = \frac{\partial \mathbf{x}}{\partial \xi} = \mathbf{r}'(\xi) + \eta \mathbf{e}'_2(\xi). \quad (65)$$

The derivative of the cross-section vector \mathbf{e}_2 with respect to ξ follows as

$$\mathbf{e}'_2 = -\theta' \mathbf{e}_1. \quad (66)$$

Thus, the rate of change of the rotation of the cross-section $\partial\theta/\partial S$, also denoted as material measure of curvature K , is given by

$$K = \frac{\partial\theta}{\partial S} = \frac{\partial\theta}{\partial\xi} \frac{\partial\xi}{\partial S} = \frac{1}{\|\bar{\mathbf{r}}'\|} \left(\frac{\mathbf{r}' \times \mathbf{r}''}{\|\mathbf{r}'\|^2} \right)^T \mathbf{e}_3. \quad (67)$$

The latter result follows from the general definition of the moment strain measure (25). In the planar case, the only nontrivial component of the vector of twist and curvature \mathbf{k} reads

$$\mathbf{k}^T \mathbf{e}_z = \frac{1}{2} \left(\mathbf{e}_1 \times \frac{\partial \mathbf{e}_1}{\partial S} + \mathbf{e}_2 \times \frac{\partial \mathbf{e}_2}{\partial S} \right)^T \mathbf{e}_z = \left(\mathbf{e}_1 \times \frac{\partial \mathbf{e}_1}{\partial S} \right)^T \mathbf{e}_z, \quad (68)$$

where the identity $\mathbf{e}_2 = \mathbf{e}_z \times \mathbf{e}_1$ has been utilized. Introducing Eq. (64) and using the relation (15), the above equation yields

$$\mathbf{k}^T \mathbf{e}_z = \left(\frac{\mathbf{r}'}{\|\mathbf{r}'\|} \times \frac{\mathbf{r}''}{\|\mathbf{r}''\|} \frac{1}{\|\bar{\mathbf{r}}'\|} \right)^T \mathbf{e}_z = \frac{1}{\|\bar{\mathbf{r}}'\|} \left(\frac{\mathbf{r}' \times \mathbf{r}''}{\|\mathbf{r}'\|^2} \right)^T \mathbf{e}_z = K. \quad (69)$$

Assuming that the beam's axis may be curved but not stretched in the undeformed configuration, i.e., $\|\bar{\mathbf{r}}'\| = 1$, we obtain the familiar relation

$$K = \left(\frac{\mathbf{r}' \times \mathbf{r}''}{\|\mathbf{r}'\|^2} \right)^T \mathbf{e}_3. \quad (70)$$

Finally, the derivative of the position vector \mathbf{x} reads

$$\mathbf{x}' = (\|\mathbf{r}'(\xi)\| - \eta K) \mathbf{e}_1. \quad (71)$$

Thus, the computation of the deformation gradient simply becomes

$$\begin{aligned} \mathbf{F} &= \frac{\partial \mathbf{x}}{\partial \xi} \otimes \mathbf{e}_1 + \frac{\partial \mathbf{x}}{\partial \eta} \otimes \mathbf{e}_2 + \mathbf{e}_3 \otimes \mathbf{e}_3 \\ &= (\|\mathbf{r}'(\xi)\| + \eta K) \mathbf{e}_1 \otimes \mathbf{e}_x + \mathbf{e}_2 \otimes \mathbf{e}_y + \mathbf{e}_3 \otimes \mathbf{e}_z. \end{aligned} \quad (72)$$

Note that the condition $\mathbf{e}_3 = \mathbf{e}_z$ holds in the planar case. It immediately follows that the only nonzero component of the Green strain tensor,

$$\mathbf{E} = \frac{1}{2}(\mathbf{F}^T \mathbf{F} - \mathbf{I}), \quad (73)$$

in the local frame $\{\mathbf{e}_1, \mathbf{e}_2, \mathbf{e}_3\}$ is given as

$$E_{11} = \frac{1}{2} \left\{ (\|\mathbf{r}'\| + \eta K)^2 - 1 \right\}. \quad (74)$$

Usually, Green's strain tensor is not used in beam theories. Its quadratic dependency on the beam's cross-section coordinate η leads to nonzero strain at the beam axis for pure bending, see Gerstmayr and Irschik (2008).

Therefore, the strain components are usually linearized with respect to the cross-section coordinates. In the planar case of Bernoulli–Euler beams, a more elegant way to obtain geometrically linearized strain measures is shown subsequently. Biot's strain tensor is obtained from the polar decomposition of the deformation gradient,

$$\mathbf{F} = \mathbf{R}\mathbf{U}, \quad (75)$$

in which \mathbf{R} denotes the rotational part of the deformation gradient and \mathbf{U} represents the stretch, which is related to Biot's strain by $\mathbf{H} = \mathbf{U} - \mathbf{I}$. Due to the simple structure of the deformation gradient in the planar case, it follows that $\mathbf{R} = \mathbf{A}$, which results in

$$\mathbf{U} = \mathbf{A}^T \mathbf{F} = (\|\mathbf{r}'\| - \eta K) \mathbf{e}_1 \otimes \mathbf{e}_x + \mathbf{e}_2 \otimes \mathbf{e}_y + \mathbf{e}_3 \otimes \mathbf{e}_z. \quad (76)$$

The work-conjugate stress to the Biot strain \mathbf{H} is the Biot stress \mathbf{B} . Under the assumption of a linear elastic material, the following relation can be applied:

$$B_{11} = E H_{11}, \quad (77)$$

in which E represents the Young's modulus.

In the beam theory, the strain component $H_{11} = \varepsilon_0 + \varepsilon_{bend}$ is split into a mean value, the (sectional) axial strain ε_0 and the bending strain proportional to the curvature K ,

$$\varepsilon_0 = \|\mathbf{r}'\| - 1 \quad \text{and} \quad \varepsilon_{bend} = \eta K. \quad (78)$$

Finally, the stress resultants are introduced as the normal force

$$N = \int_A B_{11} dA = \int_A E(\varepsilon_0 - \eta K) dA = EA\varepsilon_0, \quad (79)$$

and the bending moment

$$M = \int_A \eta \bar{B}_{11} dA = \int_A E(\eta \varepsilon_0 - \eta^2 K) dA = EI K, \quad (80)$$

where the beam's axis is chosen such that

$$\int_A E\eta dA = 0. \quad (81)$$

In order to consider curved and pre-stretched beams, the curvature \bar{K} and stretch $\bar{\varepsilon}_0$ in the undeformed configuration need to be considered,

$$N = EA(\varepsilon_0 - \bar{\varepsilon}_0), \quad M = EI(K - \bar{K}). \quad (82)$$

The relations for the sectional strain measures (78) as well as the stress resultants (82) represent the conventional linear elastic beam modeling for large deformation beams, which has been used, e.g., for the extensible Euler elastica, Reissner's shear deformable beam Reissner (1972) or the geometrically exact beam model of Simo and Vu-Quoc (1986a).

The virtual work of elastic forces for the sectional strain measures and stress resultants based on Biot's strain is provided as

$$\delta W_S = \int_L N \delta \varepsilon_0 - M \delta K d\xi. \quad (83)$$

In contrast, the St. Venant–Kirchhoff material model (29) can be used instead. The sectional strain measures as well as the stress resultants can be computed in a similar fashion from Eq. (74). For details of the derivation of the stress resultants, see Gerstmayr and Irschik (2008) and Irschik and Gerstmayr (2009b) for shear-deformable beams. The stress resultants for the St. Venant–Kirchhoff material model can be computed from the first Piola–Kirchhoff stress tensor, see Appendix A of Gerstmayr and Irschik (2008), and result in

$$N^{(P1)} = \varepsilon_{11}^0 \|\mathbf{r}'\| + \frac{3}{2} EI K^2 \|\mathbf{r}'\|, \quad (84)$$

and

$$M^{(P1)} = -EI K \|\mathbf{r}'\|^2 + \frac{1}{2} EI_4 K^3. \quad (85)$$

Obviously, the fourth area moment of inertia EI_4 enters the bending moment due to the nonlinear distribution along the cross-section of the Green–Lagrange strain, see Fig. 2 of Gerstmayr and Irschik (2008). Equations (84)–(85) provide insight into what happens in a continuum mechanics based formulation of an ANC beam finite element, which is usually based on the St. Venant–Kirchhoff material.

The virtual work of elastic forces results into the classical form

$$\delta W_S^{SVK} = \int_L N^{(P1)} \delta \varepsilon_0^{(G)} + M^{(P1)} \delta K^{(G)} d\xi, \quad (86)$$

taking into account the cross-sectional strain measures based on Green’s strain, which is indicated by a superscript ‘(G)’,

$$\varepsilon_0^{(G)} = \varepsilon_{11}^0 + \frac{1}{2} \frac{EI}{EA} K^2, \quad (87)$$

and

$$K^{(G)} = K \|\mathbf{r}'\|. \quad (88)$$

The quadratic dependency of the axial strain $\varepsilon_0^{(G)}$ on the square of the curvature K can be explained in terms of the quadratic distribution of Green’s strains, see Fig. 2 of Gerstmayr and Irschik (2008).

A comparison of Eqs. (83) and (86) reveals the difference of a continuum mechanics and a structural mechanics model of a Bernoulli–Euler beam in the ANCF. This idea can be extended to 3D and shear-deformable beams, as well. The most important contribution, however, is due to axial strain and bending.

3.3 Linearized Axial and Bending Strain and Relation to Floating Frame of Reference Formulation

The Biot’s strain component (78) corresponds to a linearization of the local strain components with respect to the local frame of the cross-section.

In the case of the Biot’s strain and Bernoulli–Euler beam theory, the polar decomposition exactly gives the rotation of the cross-section as the rotational part of the deformation gradient, cf. Eq. (76). In order to further simplify the beam finite element, it is possible to use a linearization about an average rotation of the whole beam element. Early development of the ANCF, see Shabana and Schwertassek (1997) and Escalona et al. (1998), discussed the stiffness matrix of the ANC finite element for such element-wise linearization.

A planar co-rotational coordinate system \mathbf{i} and \mathbf{j} has been introduced,

$$\mathbf{i} = \frac{\mathbf{r}^{(2)} - \mathbf{r}^{(1)}}{\|\mathbf{r}^{(2)} - \mathbf{r}^{(1)}\|}, \quad (89)$$

in which $\mathbf{r}^{(1)}$, $\mathbf{r}^{(2)}$ are the positions of the left and the right node of the finite element. The second local axis is perpendicular to \mathbf{i} , i.e.,

$$\mathbf{j} = \begin{bmatrix} -i_2 \\ i_1 \end{bmatrix}, \quad (90)$$

In this way, the vector \mathbf{u} is introduced

$$\mathbf{u} = \mathbf{r}(\xi) - \mathbf{r}^{(1)}, \quad (91)$$

and the projection of \mathbf{u} into the local element frame leads to the relations for the local beam deformation quantities

$$\mathbf{u}_d = \begin{bmatrix} u \\ v \end{bmatrix} = \begin{bmatrix} \mathbf{u}^T \mathbf{i} - \xi \\ \mathbf{u}^T \mathbf{j} \end{bmatrix}. \quad (92)$$

Thus, the strain energy can be written as

$$U = \frac{1}{2} \int_L EA u'^2 + EI v''^2 d\xi = \frac{1}{2} \int_L EA \left\{ (\mathbf{u}')^T \mathbf{i} - 1 \right\}^2 + EI \left\{ (\mathbf{u}'')^T \mathbf{j} \right\}^2 d\xi. \quad (93)$$

The latter approach fully corresponds to the floating frame of reference formulation, which assumes geometrically linearized relations in the body or element frame, see Shabana and Schwertassek (1997). An extension of this idea to shear-deformable 3D ANC beams has been introduced by Gerstmayr (2009), in which the linearized strains are computed in a co-rotational configuration of the large deformation beam element.

In a further work, a comparison of the floating frame of reference formulation based on geometrically linearized relations in each beam finite element to the ANC beam finite element with fully geometrically nonlinear formulation has been performed by Dibold et al. (2009). It turned out that co-rotationally linearized finite elements converge to exactly the same solution of large deformation static and dynamics examples as compared to Bernoulli–Euler ANC beam finite elements as discussed in the present section. The CPU performance of both formulations is similar and mainly depends on the type of mechanical problem.

3.4 Thin 3D ANC Beam Finite Element Without Torsional Stiffness

The planar Bernoulli–Euler ANC beam finite element can be extended to 3D straightforward, by adding a third component to the position and slope degrees of freedom, see Gerstmayr and Shabana (2006). In this way, a specific cable finite element is found, which has the following restrictions:

- (a) The bending stiffness must be symmetrical, $EI_{\eta\eta} = EI_{\zeta\zeta}$, which applies to homogeneous round or quadratic cables
- (b) The torsional stiffness and the moment of inertia for a rotation of the cross-section about the beam's axis is neglected; thus, it must be guaranteed that the physical problem which is modeled with the beam finite element does not show a twist or rotation about the beam's axis

If these restrictions are fulfilled, the 3D cable finite element becomes extremely simple. The axial strain is identical to the planar case (78),

$$\varepsilon_0 = \|\mathbf{r}'\| - 1, \quad (94)$$

the bending strain (material measure of curvature) is derived from Eq. (18). Due to simplicity of the structure of the rotation matrix, the formula of the curvature reads

$$K = \frac{\|\mathbf{r}' \times \mathbf{r}''\|}{\|\mathbf{r}'\|^2}. \quad (95)$$

Note that in the original work of Gerstmayr and Shabana (2006), slightly different strain measures have been used, which has been discussed and corrected in the work of Gerstmayr and Irschik (2008).

The virtual work of elastic forces for the ANC cable finite element is given by Eqs. (37) and (40), using only the axial stiffness and the bending stiffness.

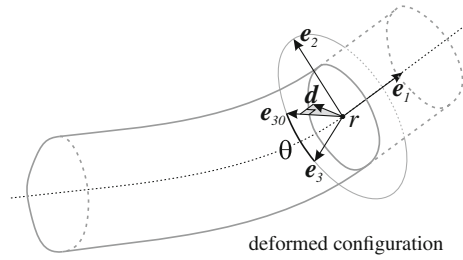
The ANC cable finite element is superior to other finite elements because of its simple structure and the resulting computational efficiency. If torsion plays an important role, however, then it needs to be extended as described in the following section.

3.5 Thin 3D ANC Beam Finite Element with Torsional Stiffness

If torsional deformation is considered additionally to bending and axial deformation of a spatial beam, then the correct representation of its configuration in space requires additional information addressing the rotation of the cross-section about the beam axis (at every point of the beam axis).

Particularly, let us choose a fixed ξ for which $\bar{\mathbf{r}}(\xi)$ and $\mathbf{r}(\xi)$ denote the position of an axial point in reference and actual configuration, respectively (see Fig. 1). The straightforward way in the ANCF to describe the rotation of a beam's cross-section at this particular point would be to consider three more absolute nodal coordinates in form of a slope vector in lateral direction, see Yakoub and Shabana (2001). However, this vector would have to yield two more conditions: first, being perpendicular to the beams axis (which is one of the basic assumptions in Bernoulli–Euler beam theory), and second, remaining its length constant in order to avoid thickness deformation of

Fig. 3 Geometrical description of a thin beam with torsional stiffness. The orientation of the cross-section at point r is defined by the normalized projection \mathbf{e}_{30} of the director \mathbf{d} into the normal plane of the beam axis, and a subsequent rotation about the beam axis by the torsional angle θ , which gives \mathbf{e}_3



the beam. Owing to that, only one degree of freedom remains to be chosen (addressing the torsional rotation of the lateral slope vector about the beam axis) in order to fully describe the beam's configuration.

We express this single degree of freedom by the natural choice of a torsional angle $\theta(\xi)$ (see Fig. 3). Note, that this angle is no more an absolute, but a relative quantity. It is measured relative to the projection of a vector $\mathbf{d}(\xi)$, called director, into the normal plane of the axial slope $\mathbf{r}'(\xi)$. The torsional angle of the cross-section in reference configuration is denoted by $\hat{\theta}(\xi)$ and measured also relative to the orientation of the director $\mathbf{d}(\xi)$, i.e., its projection into the normal plane of $\bar{\mathbf{r}}'(\xi)$. Note that the director $\mathbf{d}(\xi)$, other than the axial position or slope vectors, basically represents a constant vector in time t . Let us—for the moment, and the sake of simplicity—additionally assume, that the director is constant in space, meaning $\mathbf{d}(\xi) = \mathbf{d}$ for all ξ , and omit the explicit notion of the variables ξ and t in the following formulas. The rotation of the local frame at a particular axis point, see Eq. (6), may be defined as

$$\mathbf{e}_1 = \frac{\mathbf{r}'}{|\mathbf{r}'|}, \quad (96)$$

$$\mathbf{e}_2 = \mathbf{e}_{20} \cos(\theta) + \mathbf{e}_{30} \sin(\theta), \quad (97)$$

$$\mathbf{e}_3 = \mathbf{e}_{30} \cos(\theta) - \mathbf{e}_{20} \sin(\theta), \quad (98)$$

in which \mathbf{e}_{30} denotes the normalized projection of the director \mathbf{d} into the normal plane of the axial slope \mathbf{r}' , i.e.,

$$\mathbf{e}_{30} = \frac{\hat{\mathbf{e}}_{30}}{|\hat{\mathbf{e}}_{30}|}, \quad \hat{\mathbf{e}}_{30} = \mathbf{d} - (\mathbf{d}^T \mathbf{e}_1) \mathbf{e}_1, \quad (99)$$

and the bi-normal \mathbf{e}_{20} is obtained by the cross product

$$\mathbf{e}_{20} = \mathbf{e}_{30} \times \mathbf{e}_1. \quad (100)$$

Thereby, the curvature strain κ from Eq. (18) and the axial strain $\varepsilon_0 = \mathbf{\Gamma} \mathbf{e}_x$, utilizing $\mathbf{\Gamma}$ from Eq. (16), can be computed. Combining these strain measures together with the assumption of vanishing shear strains, i.e.,

$$|\mathbf{\Gamma}^T \mathbf{e}_y| + |\mathbf{\Gamma}^T \mathbf{e}_z| = 0,$$

the variational formulation of the strain energy according to Eq. (37) is fully defined. Note that a spatially non-constant director approach may be required combined with a temporal director update (see Sect. 3.6) in order to guarantee the Gram–Schmidt projection in Eq. (99) being well defined along the beam’s axis.

Let us turn to the spatial discretization by means of an ANC beam finite element with two nodes. In addition to the cubic interpolation of the axial position \mathbf{r} , see Eq. (62), also the torsional angle at ξ is obtained by interpolation between nodal degrees of freedom,

$$\theta(\xi) = \mathbf{S}_{m\theta}(\xi) \mathbf{q}_\theta. \tag{101}$$

The presented ANC beam finite element provides a linear interpolation of the torsional angle

$$\mathbf{S}_{m\theta}(\xi) = [S_5(\xi) \quad S_6(\xi)], \quad S_5(\xi) = \frac{1}{2} - \frac{\xi}{L}, \quad S_6(\xi) = \frac{1}{2} + \frac{\xi}{L}, \tag{102}$$

with the generalized coordinates \mathbf{q}_θ defined by the nodal values

$$\mathbf{q}_\theta = [\theta|_1 \quad \theta|_2]^T. \tag{103}$$

To prevent the element from locking, a reduced numerical integration order of 5 (e.g., via 3 point Gauß’ integration) is recommended when integrating bending and torsional stiffness terms over the beam’s axis in Eq. (37), whereas the axial stiffness term shall be integrated exact, which means a numerical integration order of 9 or higher.

3.6 Director Update

For small deformation problems it is sufficient to consider a director \mathbf{d} , which is constant in space and time. However, problems arise, if the beam’s axis, i.e., the axial slope $\mathbf{r}'(\xi)$ becomes (numerically) collinear with the director for any ξ . In this case the projection Eq. (99) becomes singular and the orientation of the beam’s cross-section remains unknown. Note that the same holds not only for the deformed configuration, but also for the undeformed configuration. As a remedy, the director is chosen to vary

1. in space, achieved, e.g., by a spatial interpolation of $\mathbf{d}(\xi)$ between the two neighboring nodal directors \mathbf{d}^1 and \mathbf{d}^2 , e.g., by a linear interpolation

$$\mathbf{d}(\xi) = S_5 \mathbf{d}^1 + S_6 \mathbf{d}^2,$$

2. in time, by performing an update of the nodal directors \mathbf{d}^1 and \mathbf{d}^2 past each time or load step, given as a function of the current orientation of the local frame at the i th node, e.g.,

$$\begin{aligned} \mathbf{d}^1(t_j) &= \mathbf{e}_{30}(\xi = -\frac{L}{2}, t = t_{j-1}), \\ \mathbf{d}^2(t_j) &= \mathbf{e}_{30}(\xi = +\frac{L}{2}, t = t_{j-1}), \end{aligned}$$

or optionally by the post-rotated update

$$\begin{aligned} \mathbf{d}^1(t_j) &= \mathbf{e}_3(\xi = -\frac{L}{2}, t = t_{j-1}), & \theta^1(t_j) &= 0 \\ \mathbf{d}^2(t_j) &= \mathbf{e}_3(\xi = +\frac{L}{2}, t = t_{j-1}), & \theta^2(t_j) &= 0 \end{aligned}$$

for all time steps t_j .

Let it be finally mentioned that the proposed Bernoulli–Euler beam finite element provides C^1 -continuity along element borders only for the geometry of the beam axis, whereas the torsion of the cross-section, i.e., angle θ , is just C^0 -continuous. Hence, the element has fourth-order convergence in problems with insignificant torsional effects, and a second-order convergence in all remaining problems. A fully C^1 continuous setting, requiring the rate of the torsional angle $\dot{\theta}$ to remain zero at the FE-nodes (in order to serve as a generalized coordinate) together with a conforming interpolation of the torsional angle θ (and the director \mathbf{d}) along the beam axis, is left for further investigation.

4 ANC Finite Elements with Shear and Cross-Section Deformation

In this section, the 2D and 3D formulations of thick ANC beam finite elements which include shear and cross-section deformation are discussed. In addition to the previous sections, displacements and displacement gradients are utilized rather than position and position gradients.

4.1 Kinematics of Thick Gradient-Deficient ANC Beam Finite Elements

Omar and Shabana (2001) presented an ANC finite element, in which a slope vector is used for modeling the shear deformation. For the 2D gradient-deficient ANC finite element, the latter finite element is modified by omitting the axial slope vector. The element is parametrized by displacements and displacement gradients at the nodes which form the degrees of freedom. Figure 2c shows a sketch of the fully parametrized element. The gradient-deficient element is obtained, if the axial slope vector $\mathbf{x}_{,\xi}$ is eliminated. The interpolation for a two-noded resp. a three-noded beam element is given with linear resp. quadratic shape functions. In case of the two-noded element, the shape functions are chosen according to Matikainen et al. (2009),

$$\begin{aligned} S_1 &= \frac{1}{L} \left(\frac{L}{2} - \xi \right), & S_2 &= \eta S_1, \\ S_3 &= \frac{1}{L} \left(\frac{L}{2} + \xi \right), & S_4 &= \eta S_3. \end{aligned} \quad (104)$$

In case of the three-noded element, the shape functions are chosen similar to those given by Mikkola et al. (2007) as

$$\begin{aligned} S_1 &= -\frac{2}{L^2} \xi \left(\frac{L}{2} - \xi \right), & S_2 &= \eta S_1, \\ S_3 &= +\frac{2}{L^2} \xi \left(\frac{L}{2} + \xi \right), & S_4 &= \eta S_3, \\ S_5 &= -\frac{4}{L^2} \left(\xi - \frac{L}{2} \right) \left(\xi + \frac{L}{2} \right), & S_6 &= \eta S_5. \end{aligned} \quad (105)$$

The 3D gradient deficient ANC beam elements can be defined as the generalization of the 2D elements discussed above. Here, the two transverse slope vectors, which are in the cross-section plane, are used as degrees of freedom, compare Fig. 2d. In the spatial case, the shape functions of the linear (two-noded) element are given by

$$\begin{aligned} S_1(\xi, \eta, \zeta) &= \frac{1}{2} - \frac{\xi}{L}, & S_2(\xi, \eta, \zeta) &= \eta S_1, & S_3(\xi, \eta, \zeta) &= \zeta S_1, \\ S_4(\xi, \eta, \zeta) &= \frac{1}{2} + \frac{\xi}{L}, & S_5(\xi, \eta, \zeta) &= \eta S_4, & S_6(\xi, \eta, \zeta) &= \zeta S_4. \end{aligned} \quad (106)$$

The shape functions for the quadratic (three-noded) ANC beam finite element are given by

$$S_1 = -\frac{2}{L^2} \xi \left(\frac{L}{2} - \xi \right), \quad S_2 = \eta S_1, \quad S_3 = \zeta S_1,$$

$$\begin{aligned}
S_4 &= +\frac{2}{L^2}\xi\left(\frac{L}{2} + \xi\right), & S_5 &= \eta S_4, & S_6 &= \zeta S_4, \\
S_7 &= -\frac{4}{L^2}\left(\xi - \frac{L}{2}\right)\left(\xi + \frac{L}{2}\right), & S_8 &= \eta S_7, & S_9 &= \zeta S_7.
\end{aligned} \tag{107}$$

4.2 Virtual Work of Elastic Forces for Thick Beams with Shear and Cross-Section Deformation

In addition to the structural mechanics formulation, which is customary for thin beams, a structural as well as a continuum mechanics based formulation is provided for shear and cross-section deformable ANC finite elements. Following the work of Gerstmayr et al. (2008), the work of elastic forces can be based on Reissner's nonlinear rod theory, see Reissner (1972), as implemented by Simo and Vu-Quoc (1986a), and a continuum mechanics based formulation, using a St. Venant–Kirchhoff material. For the 3D case, see Nachbagauer et al. (2011).

4.2.1 Continuum Mechanics Formulation

In the original shear-deformable ANC beam finite element by Omar and Shabana (2001), the elastic strain energy is defined using the Green's strain and the second Piola–Kirchhoff stress, as provided in Eq. (28). The main problem of this original continuum mechanics based formulation is the Poisson-locking phenomenon. In the original approach, the strain energy of a beam element with a rectangular cross-section is written in terms of the engineering strain vector $\bar{\epsilon}$ and the elasticity matrix $\bar{\mathbf{D}}_{\text{CM}}$ as presented in Eq. (33). The main problem of the original continuum mechanics based formulation arises since the Poisson ratio ν couples axial strains \bar{E}_{11} and transverse normal strains \bar{E}_{22} in the stress-strain relation. For pure axial deformation, the Poisson effect is modeled exactly. However, for bending deformation, the Poisson effect would require a trapezoidal deformation of the cross-section, which is not available in the original formulation. To avoid the locking effect, the strain energy is modified based on the idea of Gerstmayr et al. (2008). The elasticity matrix is split into two parts:

$$\bar{\mathbf{D}}_{\text{CM}} = \bar{\mathbf{D}}_{\text{CM}}^0 + \bar{\mathbf{D}}_{\text{CM}}^\nu, \tag{108}$$

in which $\bar{\mathbf{D}}_{\text{CM}}^0$ does not include the Poisson ratio ν , while $\bar{\mathbf{D}}_{\text{CM}}^\nu$ involves the Poisson effect only. Hereafter, the strain energy is integrated over the cross-section, see Eq. (28), in which the part related to $\bar{\mathbf{D}}_{\text{CM}}^0$ is integrated over the cross-section and the other part related to $\bar{\mathbf{D}}_{\text{CM}}^\nu$ is integrated along the beam axis only using the cross-sectional area.

4.2.2 Structural Mechanics Formulation

The idea of the structural mechanics formulation is to incorporate the strain energy of classical nonlinear rod theories into the ANCF, for details see Gerstmayr et al. (2008) and Nachbagauer et al. (2011). The planar case of Eq. (37) reads

$$\delta W^{\text{int}} = \int_L EA \bar{\Gamma}_1 \delta \bar{\Gamma}_1 + k_s GA \bar{\Gamma}_2 \delta \bar{\Gamma}_2 + EI \bar{\kappa} \delta \bar{\kappa} d\xi, \quad (109)$$

in which the axial stiffness EA , the shear stiffness GA with the shear correction factor k_s , and the bending stiffness EI are coupled to the generalized strain measures for axial, shear, and bending strains, respectively. As proposed by Simo and Vu-Quoc (1986a), shear locking is eliminated by means of reduced integration here.

An additional term in the strain energy is necessary regarding the degrees of freedom of the cross-section deformation. Following Gerstmayr et al. (2008), the additional thickness strain energy $W_{\text{cs}}^{\text{int}}$ in case of a 2D beam finite element can be defined—in case of a rectangular cross-section—by

$$\delta W_{\text{cs}}^{\text{int}} = \int_L EA \bar{E}_{22} \delta \bar{E}_{22} d\xi, \quad (110)$$

which is defined similar to Eq. (48). The enhanced strain energy in the structural mechanics based formulation is the sum of the conventional strain energy W^{int} in Eq. (109) and $W_{\text{cs}}^{\text{int}}$ in Eq. (110), see Eq. (37). In the 3D case, the structural mechanics based formulation follows Simo (1985). For the case of simple symmetric cross-sections, see Eqs. (42) and (37) can be given for the single components,

$$\begin{aligned} \delta W^{\text{int}} = \int_L & EA \bar{\Gamma}_1 \delta \bar{\Gamma}_1 + GA k_2 \bar{\Gamma}_2 \delta \bar{\Gamma}_2 + GA k_3 \bar{\Gamma}_3 \delta \bar{\Gamma}_3 \\ & + G J k_t \bar{\kappa}_1 \delta \bar{\kappa}_1 + EI_2 \bar{\kappa}_2 \delta \bar{\kappa}_2 + EI_3 \bar{\kappa}_3 \delta \bar{\kappa}_3 d\xi. \end{aligned} \quad (111)$$

In the 3D case, the virtual work of elastic forces covering cross-section deformation follows from Eq. (48).

5 Evaluation of the Accuracy and Performance of ANC Finite Elements

This section is dedicated to outline the numerical behavior of four of the proposed ANC beam finite elements, all of which are implemented in the open-source flexible multibody system dynamics code HOTINT,² see Gerstmayr et al. (2013a). Henceforth, let us use abbreviations as in Table 1.

²<http://www.hotint.org/>.

The interested reader is referred to the works by Gerstmayr and Irschik (2008), Gerstmayr et al. (2008), Nachbagauer et al. (2011), Nachbagauer et al. (2013) and Gruber et al. (2013), in which each of the proposed ANC beam finite elements is tested separately.

5.1 Static Example (Planar): Largely Deforming Cantilever

In this example we aim to compare the convergence and performance properties of all proposed ANC beam finite elements (Table 1) at once, i.e., both thin and thick elements are studied on behalf of the same setup.

A cantilever with length L and square cross-section with side-length a is subjected to a point load \mathbf{F} acting at the material point B (which is the tip of the beam axis, see Fig. 4). The material parameters of the cantilever are defined by Young’s modulus E and Poisson’s ratio ν as

$$E = 2.07 \times 10^{11} \text{ N/m}^2, \quad \nu = 0.3,$$

based on which the shear modulus G and the shear correction factor k_s are given by

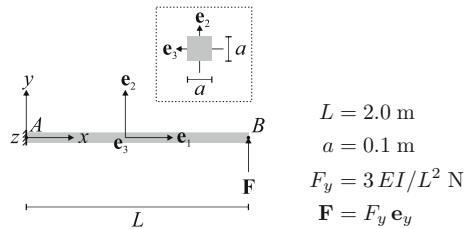
$$G = \frac{E}{2(\nu + 1)} \text{ N/m}^2, \quad k_s = \frac{10(1 + \nu)}{12 + 11\nu}. \quad (112)$$

Table 1 Types of ANC beam finite elements tested in Sect. 5

| Name | Theory | Description |
|------|-----------|--------------------------------------------------|
| BE2D | Sect. 3 | Thin beam in 2D (acc. to Bernoulli–Euler theory) |
| BE3D | Sect. 3.5 | Same in 3D |
| SQ2D | Sect. 4 | Shear deformable beam in 2D |
| SQ3D | Sect. 4 | Same in 3D |

Throughout the whole section the shear-deformable ANC beam finite elements SQ2D and SQ3D are considered to use quadratic shape functions, as defined in Eq. (105)

Fig. 4 Geometrical setup of the cantilever of Sect. 5.1 in reference configuration



A reference solution to the problem has been computed in the mathematical software framework Maple by solving an elliptic integral equation utilizing global polynomial shape functions, see Gerstmayr and Irschik (2008). The respective polynomial degree was chosen such that the first 12 digits of the displacement at material point B , reading

$$\mathbf{u}_{\text{ref}}^B = \begin{cases} -0.50853730436 \mathbf{e}_x + 1.20723985455 \mathbf{e}_y, & \text{for BE2D and BE3D,} \\ -0.50946471774 \mathbf{e}_x + 1.20882282955 \mathbf{e}_y, & \text{for SQ2D and SQ3D,} \end{cases} \quad (113)$$

have been converged.

All of the four beams, cf. Table 1, were tested in a scenario with ten uniform load steps, i.e.,

$$\mathbf{F}_i = \frac{i}{10} \mathbf{F}.$$

At each of those load steps a nonlinear system is solved by means of Newton’s method, utilizing the solution of the previous load step as initial guess at the current load step. Newton’s method is terminated if the relative error (i.e., max-norm of the actual residual over max-norm of the initial residual) becomes less than the bound $\varepsilon = 10^{-8}$. The overall performance and convergence behavior of the respective ANC beam finite elements are documented in Table 2 as well as in the convergence plots of Fig. 5 and a performance plot in Fig. 6.

Studying these tables and figures we arrive at the following conclusions:

1. All of the elements of Table 1 require roughly the same number of Newton iterations, independently of the underlying spatial refinement level.
2. Comparing the error of tip deflection $|\mathbf{u}_{\text{ref}}^B - \mathbf{u}_{\text{FE}}^B|$ versus number of elements (see also the left plot in Fig. 2), a quantitatively slightly different, but asymptotically equal behavior of all element types can be observed, namely a convergence order of 4 (meaning a decrease of the error roughly by a factor of c^{-4} if the number of elements is increased by a factor of $c > 0$).
3. The right plot in Fig. 2 seems to be a consequence from the left plot, owing to the fact that thick (i.e., shear-deformable) beam elements naturally own more degrees of freedom than their thin counterparts. The same holds of course with respect to the dimensionality of the several beam types.
4. The final plot in Fig. 6 shows that thin and thick elements need roughly the same computational time asymptotically, both in the planar and in the spatial case.

5.2 Free Beam Flying in Plane

By this planar dynamic benchmark example we aim to compare the computational speed of all the ANC finite elements presented in Table 1, as well as their convergence in terms of a displacement error, integrated over time.

Table 2 Performance table for the example *Largely deforming cantilever* of Sect. 5.1

| Spatial discretization | | | Performance | |
|------------------------|------|------------|-------------|-------|
| #NEL | #DOF | Err. (m) | CPU (s) | #Its. |
| SQ2D | | | | |
| 1 | 12 | 1.098e-001 | 0.109 | 51 |
| 2 | 20 | 1.516e-002 | 0.187 | 49 |
| 4 | 36 | 1.327e-003 | 0.297 | 49 |
| 8 | 68 | 9.159e-005 | 0.531 | 49 |
| 16 | 132 | 5.874e-006 | 0.952 | 49 |
| 32 | 260 | 3.695e-007 | 1.731 | 49 |
| 64 | 516 | 2.312e-008 | 3.244 | 50 |
| BE2D | | | | |
| 1 | 8 | 2.585e-001 | 0.094 | 49 |
| 2 | 12 | 3.755e-002 | 0.156 | 49 |
| 4 | 20 | 2.035e-003 | 0.265 | 49 |
| 8 | 36 | 5.060e-005 | 0.655 | 49 |
| 16 | 68 | 1.202e-006 | 0.827 | 49 |
| 32 | 132 | 3.876e-008 | 1.716 | 49 |
| 64 | 260 | 1.820e-009 | 3.136 | 49 |
| SQ3D | | | | |
| 1 | 27 | 1.098e-001 | 1.482 | 54 |
| 2 | 45 | 1.516e-002 | 2.324 | 55 |
| 4 | 81 | 1.327e-003 | 4.586 | 55 |
| 8 | 153 | 9.159e-005 | 8.471 | 55 |
| 16 | 297 | 5.874e-006 | 16.41 | 55 |
| 32 | 585 | 3.695e-007 | 32.6 | 55 |
| 64 | 1161 | 2.312e-008 | 70.86 | 55 |
| BE3D | | | | |
| 1 | 14 | 2.585e-001 | 0.905 | 49 |
| 2 | 21 | 3.755e-002 | 1.404 | 49 |
| 4 | 35 | 2.035e-003 | 2.652 | 49 |
| 8 | 63 | 5.060e-005 | 4.695 | 49 |
| 16 | 119 | 1.202e-006 | 9.002 | 49 |
| 32 | 231 | 3.876e-008 | 17.94 | 49 |
| 64 | 455 | 1.820e-009 | 35.47 | 49 |

CPU-time in seconds (CPU (s)) and number of Newton iterations (#Its.) for various levels of spatial approximation including number of elements (#NEL), total degrees of freedom (#DOF), and approximation error (Err. (m)), measured by the error of the tip deflection, i.e. $\text{Err.} = |\mathbf{u}_{\text{ref}}^{\text{B}} - \mathbf{u}_{\text{FE}}^{\text{B}}|$

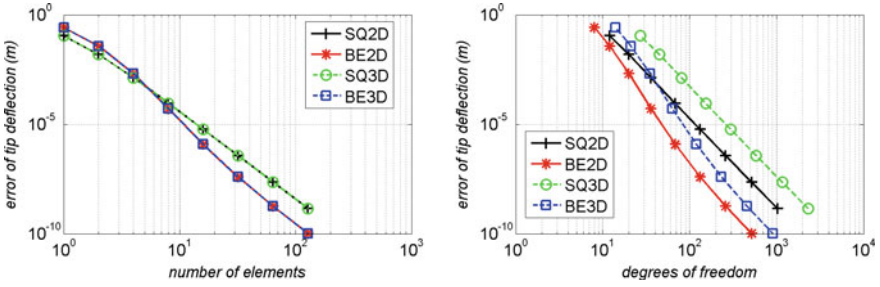


Fig. 5 Convergence plot of the example problem in Sect. 5.1 showing the error of tip deflection $|\mathbf{u}_{\text{ref}}^B - \mathbf{u}_{\text{FE}}^B|$ versus number of elements (*left*) and degrees of freedom (*right*)

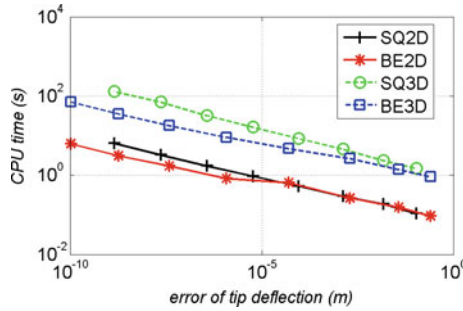


Fig. 6 The performance of the ANC beam finite elements in the example problem of Sect. 5.1 is compared in terms of CPU-time versus error of tip deflection $|\mathbf{u}_{\text{ref}}^B - \mathbf{u}_{\text{FE}}^B|$

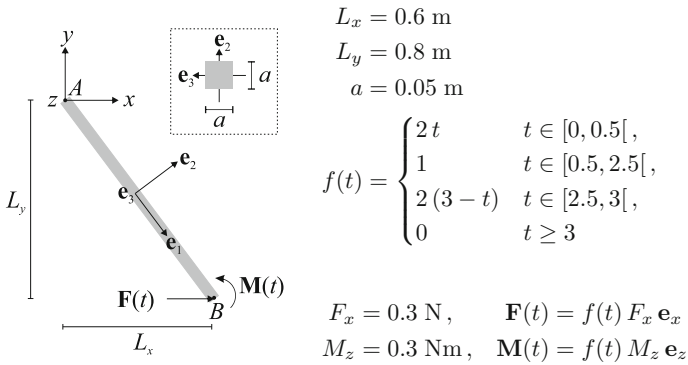


Fig. 7 Geometrical setup of the free beam of Sect. 5.2 in reference configuration

A free beam with a square cross-section, as shown in Fig. 7, is subjected to a force $\mathbf{F}(t)$ and a moment $\mathbf{M}(t)$, both acting over the time $t \in [0, 10]$ at the beam axis point B . The material parameters of the beam are defined by Young's modulus E , Poisson's ratio ν , and the material density ρ as

$$E = 1 \times 10^5 \text{ N/m}^2, \quad \nu = 0.3, \quad \rho = 2500 \text{ kg/m}^3, \quad (114)$$

based on which the shear modulus G and the shear correction factor k_s are computed up to double precision, utilizing Eq. (112).

Note that the problem setup is defined similar but not equal to the well-known *flying spaghetti problem* of Simo and Vu-Quoc (1986b). The reason for considering not the original but a modified problem setup is to end up with less differences in the kinematic behavior of thin and shear-deformable beam elements.

Time integration is numerically performed by a uniform time step size $\Delta t = 0.001$ s utilizing a two staged trapezoidal rule (Lobatto), which means three integration points per time step and a fourth-order global convergence in time. In difference to the test example *largely deforming cantilever* of Sect. 5.1, where a classical Newton method was used per load step, we choose to update the Jacobian not at each time step, but only if required, i.e., if the Newton residual is not converging fast enough. Although generally resulting in much more iteration steps, such a modified Newton method speeds up the simulation, particularly if the considered time steps are comparatively small. Alike the classical Newton method, the modified Newton method is terminated, if the relative error (i.e., max-norm of the actual residual over max-norm of the initial residual) becomes less than the bound $\varepsilon = 10^{-8}$.

Two convergence plots in Fig. 8 and a performance plot in Fig. 9 conclude this example. In all of these plots, the integrated deflection error

$$\epsilon_T = \left(\int_0^T |\mathbf{u}_{\text{ref}}^B - \mathbf{u}_{\text{FE}}^B|^2 dt \right)^{1/2} \quad (115)$$

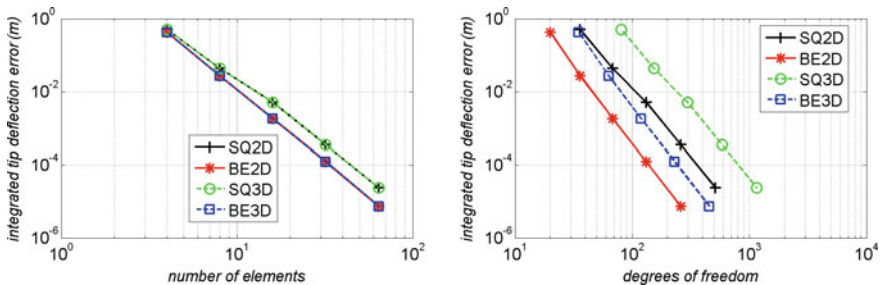
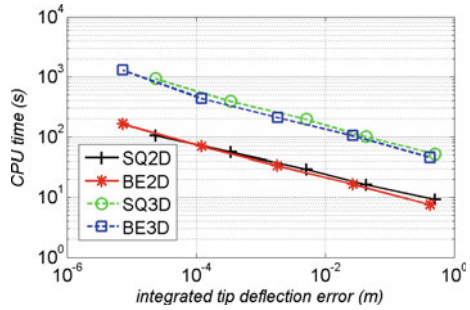


Fig. 8 Convergence plot of the example problem in Sect. 5.2 showing the integrated tip deflection error, as defined in Eq. (115), versus number of elements (*left*) or degrees of freedom (*right*)

Fig. 9 The performance of the ANC beam finite elements in the example problem of Sect. 5.2 is compared in terms of CPU-time versus integrated tip deflection error, as defined in Eq. (115)



at material point B (see Fig. 7) served as a measure of the finite element approximation error. The reference solution \mathbf{u}_{ref}^B (which is different for thin and for shear deformable beams) is computed by means of a highly refined FE-solution of 128 elements, also at a time step size of $\Delta t = 0.001$ s.

5.3 Free Beam Flying in Space

If a spatial beam formulation uses angular in addition to absolute coordinates (which is the case in the beam class BE3D, but not so in the beam class SQ3D), the shape function interpolation of those angular coordinates (evaluated at the integration points along the beam’s axis) causes the total energy of the beam to be no more conserved, and thus any time integration scheme becomes unstable and must fail to converge. To demonstrate this effect in this third test example, we consider a similar problem setup as in Sect. 5.2, however with slightly different material and geometrical parameters, and with a different loading scenario causing the beam to move out of plane.

A free beam with a square cross-section, as shown in Fig. 10, is subjected to a moment $\mathbf{M}(t)$ acting at the time t at the beam axis point B . The material parameters of the beam are defined by Young’s modulus E , Poisson’s ratio ν , and the material density ρ as in Eq. (114), based on which the shear modulus G and the shear correction factor k_s are computed up to double precision, utilizing Eq. (112).

Although the beam class BE3D shows better convergence compared to the beam class SQ3D (as shown in Fig. 12) the simulation with type BE3D elements would become unstable after a while. To be precise, an implicit time integration scheme (of type Lobatto using 2 stages and a uniform time step size of 0.001 s) would fail to converge after 8 s of simulation time when using a spatial discretization with 8 elements, after 9 s when using 16 elements, and after 12 s when using 32 elements

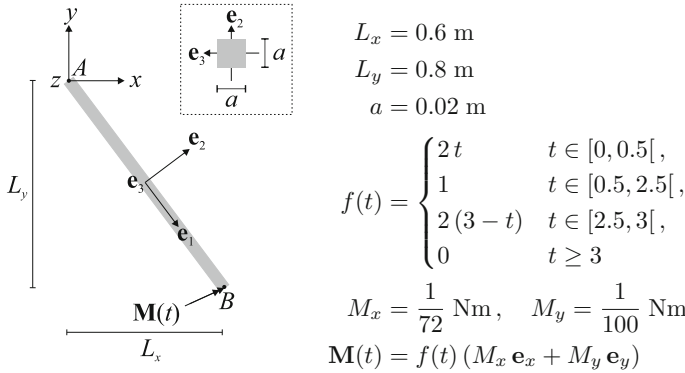


Fig. 10 Geometrical setup of the free beam of Sect. 5.3 in reference configuration

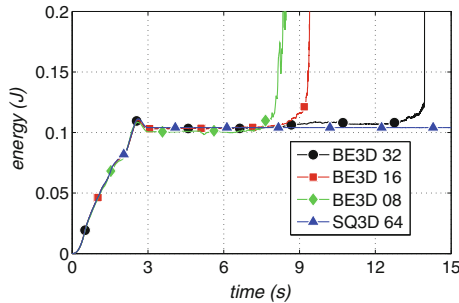


Fig. 11 Sum of kinetic and potential energy of the beam computed with a uniform time step of 0.001 s and a spatial discretization of 8, 16, and 32 elements of type BE3D compared to 64 elements of type SQ3D

of beam type BE3D, whereas simulations with the same type of integration scheme but using SQ3D elements did not show instability effects at all (at least, in our tests the simulation remained stable until 50 s of simulation time).

This issue becomes even more evident if we study the total (i.e., the sum of kinetic and potential) energy, see Fig. 11. Analytically the total energy of the flying beam must stay constant as soon as the outer forces, i.e., the tip moment, become zero (which happens past 3 s of simulation time, see the definition of the time ramp $f(t)$ in Fig. 10). In case of simulations with BE3D elements, sudden energy blowups occur whereas in simulations with SQ3D elements the total energy is conserved, independently of the spatial refinement.

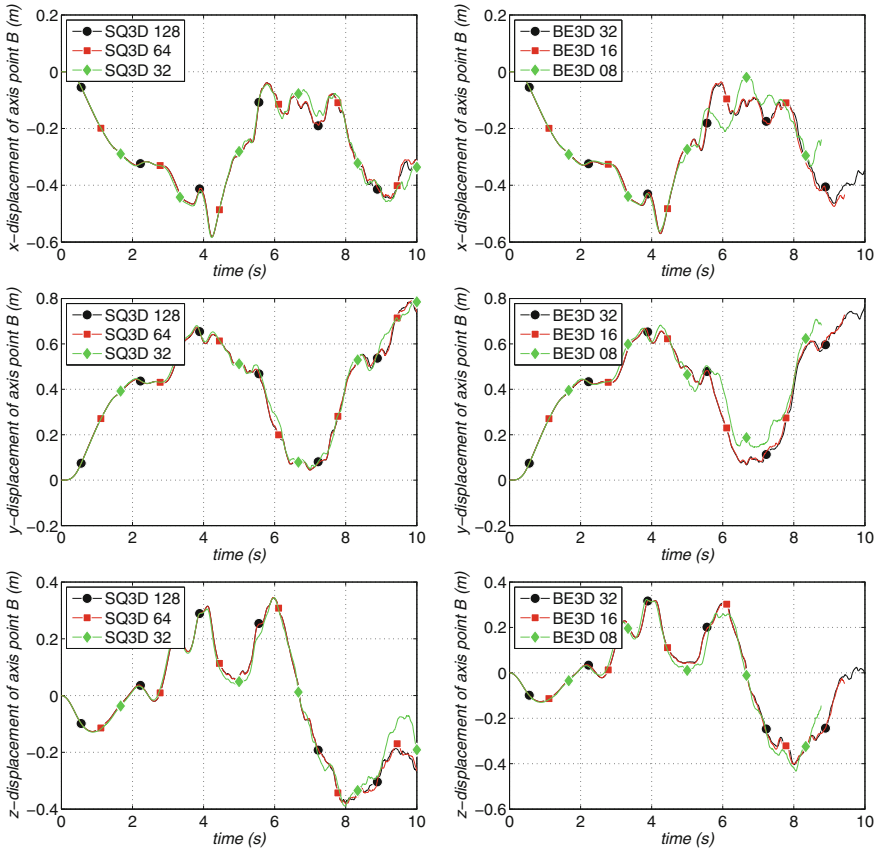


Fig. 12 Displacement in x -, y -, and z -direction of the axial point B of the beam in Sect. 5.3 computed with 32, 64, and 128 elements of type SQ3D (left), and 8, 16, and 32 elements of type BE3D (right)

6 Conclusions

In the present chapter, the absolute nodal coordinate formulation has been introduced and some specific finite elements, which are based upon this formulation, have been presented in a unified notation regarding kinematics and work of elastic forces. The finite elements under investigation have been studied regarding its convergence as well as the stability. It turned out that displacement-based finite elements, which do not employ rotations as degrees of freedom, are not showing numerical instabilities as compared to those which contain at least one rotational parameter. Finite elements with rotational parameters, however, have other advantages. For those elements, it is necessary to obtain stable numerical integration schemes, which are discussed in detail in other chapters of this book.

Acknowledgments The authors Gerstmayr, Humer, and Gruber have been supported by the Linz Center of Mechatronics (LCM) in the framework of the Austrian Comet-K2 programme. K. Nachbagauer acknowledges support from the Austrian Science Fund (FWF): T733-N30.

References

- Antman, S. S. (1972). The theory of rods. In S. Flügge & C. Truesdell (Eds.), *Handbuch der Physik* (Vol. VIa/2, pp. 641–703). Berlin: Springer.
- Berzeri, M., & Shabana, A. A. (2002). Development of simple models for the elastic forces in the absolute nodal co-ordinate formulation. *Journal of Sound and Vibration*, 235(4), 539–565.
- Betsch, P., & Steinmann, P. (2003). Constrained dynamics of geometrically exact beams. *Computational Mechanics*, 31, 49–59.
- Dibold, M., Gerstmayr, J., & Irschik, H. (2009). A detailed comparison of the absolute nodal coordinate and the floating frame of reference formulation in deformable multibody systems. *ASME Journal of Computational and Nonlinear Dynamics*, 4(2), 10.
- Dmitrochenko, O. N., & Pogorelov, D. Y. (2003). Generalization of plate finite elements for absolute nodal coordinate formulation. *Multibody System Dynamics*, 10, 17–43. <http://dx.doi.org/10.1023/A:1024553708730>. ISSN: 1384-5640.
- Escalona, J. L., Hussien, H. A., & Shabana, A. A. (1998). Application of the absolute nodal coordinate formulation to multibody system dynamics. *Journal of Sound and Vibration*, 214(5), 833–851.
- Frischkorn, J., & Reese, S. (2012). A novel solid-beam finite element for the simulation of nitinol stents. In *Proceedings of the ECCOMAS 2012 European Congress on Computational Methods on Applied Sciences and Engineering, Vienna, Austria*.
- Gerstmayr, J. (2009). A corotational approach for 3D absolute nodal coordinate elements. In *Proceedings of the ASME IDETC/CIE 2009, San Diego, USA*.
- Gerstmayr, J., & Irschik, H. (2003). Vibrations of the elasto-plastic pendulum. *International Journal of Nonlinear Mechanics*, 38, 111–122.
- Gerstmayr, J., & Irschik, H. (2008). On the correct representation of bending and axial deformation in the absolute nodal coordinate formulation with an elastic line approach. *Journal of Sound and Vibration*, 318, 461–487.
- Gerstmayr, J., & Matikainen, M. K. (2006). Analysis of stress and strain in the absolute nodal coordinate formulation. *Mechanics Based Design of Structures and Machines*, 34, 409–430.
- Gerstmayr, J., & Shabana, A. A. (2006). Analysis of thin beams and cables using the absolute nodal coordinate formulation. *Nonlinear Dynamics*, 45(1–2), 109–130.
- Gerstmayr, J., Matikainen, M. K., & Mikkola, A. M. (2008). A geometrically exact beam element based on the absolute nodal coordinate formulation. *Journal of Multibody System Dynamics*, 20, 359–384.
- Gerstmayr, J., Doringner, A., Eder, R., Gruber, P., Reischl, D., Saxinger, M., Schörgenhumer, M., Humer, A., Nachbagauer, K., Pechstein, A., & Vetyukov, Y. (2013a). Hotint: A script language based framework for the simulation of multibody dynamics systems. In *9th International Conference on Multibody Systems, Nonlinear Dynamics, and Control* (Vol. 7B). doi:10.1115/DETC2013-12299.
- Gerstmayr, J., Sugiyama, H., & Mikkola, A. (2013b). Review on the absolute nodal coordinate formulation for large deformation analysis of multibody systems. *ASME Journal of Computational and Nonlinear Dynamics*, 8, 031016 (12 pages).
- Gruber, P. G., Nachbagauer, K., Vetyukov, Y., & Gerstmayr, J. (2013). A novel director-based Bernoulli-Euler beam finite element in absolute nodal coordinate formulation free of geometric singularities. *Mechanical Sciences*, 4(2), 279–289. doi:10.5194/ms-4-279-2013. <http://www.mech-sci.net/4/279/2013/>.

- Irschik, H., & Gerstmayr, J. (2009a). A hyperelastic Reissner-type model for non-linear shear deformable beams. In I. Troch & F. Breiteneker (Eds.), *Proceedings of the Mathmod 09*.
- Irschik, H., & Gerstmayr, J. (2009b). A continuum mechanics based derivation of Reissner's large-displacement finite-strain beam theory: The case of plane deformations of originally straight Bernoulli-Euler beams. *Acta Mechanica*, 206, 1–21.
- Irschik, H., & Gerstmayr, J. (2011). A continuum-mechanics interpretation of Reissner's non-linear shear-deformable beam theory. *Mathematical and Computer Modelling of Dynamical Systems*, 17(1), 19–29.
- Lan, P., & Shabana, A. (2010a). Integration of B-spline geometry and ANCF finite element analysis. *Nonlinear Dynamics*, 61(1–2), 193–206.
- Lan, P., & Shabana, A. (2010b). Rational finite elements and flexible body dynamics. *ASME Journal of Vibration and Acoustics*, 132(4), 041007.
- Matikainen, M. K., von Hertzen, R., Mikkola, A., & Gerstmayr, J. (2009). Elimination of high frequencies in the absolute nodal coordinate formulation. In *Proceedings of the Institution of Mechanical Engineers, Part K, Journal of Multi-body Dynamics*.
- Mikkola, A. M., & Shabana, A. A. (2003). A non-incremental finite element procedure for the analysis of large deformations of plates and shells in mechanical system applications. *Multibody System Dynamics*, 9, 283–309.
- Mikkola, A. M., Garcia-Vallejo, D., & Escalona, J. L. (2007). A new locking-free shear deformable finite element based on absolute nodal coordinates. *Nonlinear Dynamics*, 50, 249–264.
- Nachbagauer, K., Pechstein, A. S., Irschik, H., & Gerstmayr, J. (2011). A new locking-free formulation for planar, shear deformable, linear and quadratic beam finite elements based on the absolute nodal coordinate formulation. *Multibody System Dynamics*, 26, 245–263.
- Nachbagauer, K., Gruber, P., & Gerstmayr, J. (2013). Structural and continuum mechanics approaches for a 3D shear deformable ANCF beam finite element: Application to static and linearized dynamic examples. *Journal of Computational and Nonlinear Dynamics*, 8, 021004.
- Olshvskiy, A., Dmitrochenko, O., & Kim, C.-W. (2013). Three-dimensional solid brick element using slopes in the absolute nodal coordinate formulation. *Journal of Computational and Nonlinear Dynamics*, 9(2), 021001.
- Omar, M. A., & Shabana, A. A. (2001). A two-dimensional shear deformable beam for large rotation and deformation problems. *Journal of Sound and Vibration*, 243(3), 565–576.
- Pechstein, A., & Gerstmayr, J. (2013). A Lagrange-Eulerian formulation of an axially moving beam based on the absolute nodal coordinate formulation. *Multibody System Dynamics*, 30(3), 343–358.
- Reissner, E. (1972). On one-dimensional finite-strain beam theory: The plane problem. *Journal of Applied Mathematics and Physics*, 23, 795–804.
- Reissner, E. (1973). On one-dimensional large-displacement finite-strain beam theory. *Studies in Applied Mathematics*, 11, 1(2), 87–95.
- Shabana, A. A., & Schwertassek, R. (1997). Equivalence of the floating frame of reference approach and finite element formulations. *International Journal of Non-Linear Mechanics*, 33(3), 417–432.
- Simo, J. C. (1985). A finite strain beam formulation. The three-dimensional dynamic problem. Part I. *Computer Methods in Applied Mechanics and Engineering*, 49, 55–70.
- Simo, J. C., & Vu-Quoc, L. (1986a). On the dynamics of flexible beams under large overall motions—the plane case: Part I. *Journal of Applied Mechanics*, 53(4), 849–854. doi:10.1115/1.3171870. <http://dx.doi.org/10.1115/1.3171870>. ISSN: 0021-8936.
- Simo, J. C., & Vu-Quoc, L. (1986b). On the dynamics of flexible beams under large overall motions—the plane case: Part II. *Journal of Applied Mechanics*, 53(4), 855–863. doi:10.1115/1.3171871. <http://dx.doi.org/10.1115/1.3171871>. ISSN: 0021-8936.
- Simo, J. C., & Vu-Quoc, L. (1986c). A three-dimensional finite-strain rod model. Part II: Computational aspects. *Computer Methods in Applied Mechanics and Engineering*, 58, 79–116.
- Simo, J. C., & Vu-Quoc, L. (1988). On the dynamics in space of rods undergoing large motions—a geometrically exact approach. *Computer Methods in Applied Mechanics and Engineering*, 66, 125–161.

- Sugiyama, H., & Shabana, A. A. (2004). Application of plasticity theory and absolute nodal coordinate formulation to flexible multibody system dynamics. *ASME Journal of Mechanical Design*, *126*, 478–487.
- Sugiyama, H., Escalona, J. L., & Shabana, A. A. (2003). Formulation of three-dimensional joint constraints using the absolute nodal coordinates. *Nonlinear Dynamics*, *31*, 167–195.
- Yakoub, R. Y., & Shabana, A. A. (2001). Three dimensional absolute nodal coordinate formulation for beam elements. *ASME Journal of Mechanical Design*, *123*, 606–621.